Science of the Total Environment 870 (2023) 161644

Contents lists available at ScienceDirect

Science of the Total Environment

journal homepage: www.elsevier.com/locate/scitotenv

Climate impacts on tree-ring stable isotopes across the Northern Hemispheric boreal zone

Olga V. Churakova (Sidorova) [a,b,c,*], Trevor J. Porter [d], Mikhail S. Zharkov [a], Marina V. Fonti [b], Valentin V. Barinov [a], Anna V. Taynik [a], Alexander V. Kirdyanov [a,e], Anastasya A. Knorre [a,f], Martin Wegmann [g], Tatyana V. Trushkina [h], Nataly N. Koshurnikova [a], Eugene A. Vaganov [a,e], Vladimir S. Myglan [a], Rolf T.W. Siegwolf [b], Matthias Saurer [b,*]

[a] Siberian Federal University, 660041 Svobodny 79, Krasnoyarsk, Russian Federation
[b] Swiss Federal Institute for Forest, Snow and Landscape Research WSL, Zürcherstrasse 111, CH-8903 Birmensdorf, Switzerland
[c] Kasan Federal University, Institute of Geology and Petroleum Technology, Kremlyovskaya str. 18, Kazan 420008, Russian Federation
[d] Department of Geography, Geomatics and Environment, University of Toronto Mississauga, 3359 Mississauga Road, Mississauga, ON L5L 1C6, Canada
[e] Sukachev Institute of Forest SB RAS, Federal Research Center 'Krasnoyarsk Science Center SB RAS', 660036 Krasnoyarsk, Akademgorodok, Russian Federation
[f] Science Department, National Park "Krasnoyarsk Stolby", 660006 Krasnoyarsk, Russian Federation
[g] École Polytechnique Fédérale de Lausanne EPFL, Limnology center, 1015 Lausanne, Switzerland
[h] Reshetnev Siberian State University of Science and Technology, Krasnoyarsky Rabochy 31, 660037 Krasnoyarsk, Russian Federation

HIGHLIGHTS

- First Boreal network of triple tree-ring stable isotopes from 6 conifer tree species.
- Winter-spring air temperatures is recorded by oxygen isotopes.
- Solar irradiation is recorded in tree-ring hydrogen isotopes.
- Both $\delta^{18}O_{trc}$ and $\delta^{2}H_{trc}$ are recording ecohydrological signal at the tree level.
- Wet conditions for Scandinavia concurrent with drier anomalies in Canada and Siberia.

GRAPHICAL ABSTRACT

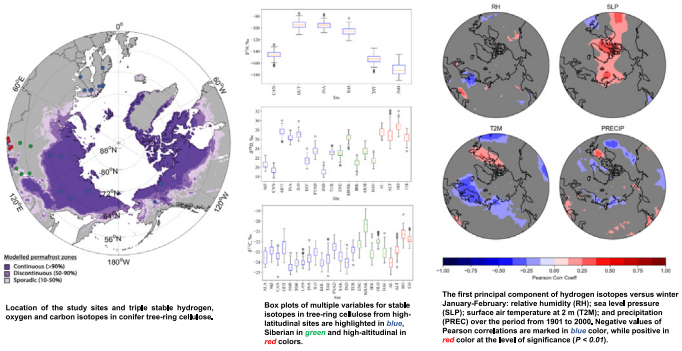

ARTICLE INFO

Editor: Elena Paoletti

Keywords:
Stable isotopes in tree-ring cellulose
Water isotopes
Climate transects
Oscillation patterns
Sea level pressure
Permafrost

ABSTRACT

Boreal regions are changing rapidly with anthropogenic global warming. In order to assess risks and impacts of this process, it is crucial to put these observed changes into a long-term perspective. Summer air temperature variability can be well reconstructed from conifer tree rings. While the application of stable isotopes can potentially provide complementary climatic information over different seasons.

In this study, we developed new triple stable isotope chronologies in tree-ring cellulose ($\delta^{13}C_{trc}$, $\delta^{18}O_{trc}$, $\delta^{2}H_{trc}$) from a study site in Canada. Additionally, we performed regional aggregated analysis of available stable isotope chronologies from 6 conifers' tree species across high-latitudinal (HL) and - altitudinal (HA) as well as Siberian (SIB) transects of the Northern Hemispheric boreal zone.

Our results show that summer air temperature still plays an important role in determining tree-ring isotope variability at 11 out of 24 sites for $\delta^{13}C_{trc}$, 6 out of 18 sites for $\delta^{18}O_{trc}$ and 1 out of 6 sites for $\delta^{2}H_{trc}$. Precipitation, relative humidity and vapor pressure deficit are significantly and consistently recorded in both $\delta^{13}C_{trc}$ and $\delta^{18}O_{trc}$ along HL.

Summer sunshine duration is captured by all isotopes, mainly for HL and HA transects, indicating an indirect link with an increase in air and leaf temperature. A mixed temperature-precipitation signal is preserved in $\delta^{13}C_{trc}$ and $\delta^{18}O_{trc}$

* Correspondence to: O.V. Churakova (Sidorova), Siberian Federal University, 660041 Svobodny 79, Krasnoyarsk, Russian Federation; M. Saurer, Swiss Federal Institute for Forest, Snow and Landscape Research WSL, Zürcherstrasse 111 CH-8903 Birmensdorf, Switzerland.
E-mail addresses: ochurakova@sfu-kras.ru (O.V. Churakova (Sidorova)), matthias.saurer@wsl.ch (M. Saurer).

http://dx.doi.org/10.1016/j.scitotenv.2023.161644
Received 18 December 2022; Received in revised form 10 January 2023; Accepted 12 January 2023
Available online 24 January 2023

along SIB transect. The δ^2H_{trc} data obtained for HL-transect provide information not only about growing seasonal moisture and temperature, but also capture autumn, winter and spring sunshine duration signals. We conclude that a combination of triple stable isotopes in tree-ring studies can provide a comprehensive description of climate variability across the boreal forest zone and improve ecohydrological reconstructions.

1. Introduction

The Northern Hemispheric boreal zone represents a huge range of forest distribution from 50 to 70° N (Apps et al., 2006). In northern Canada, central and northeastern Siberia, large areas of the boreal forest also overlap with the continuous permafrost zone, which due to increasing temperature, may thaw rapidly and unlock additional organic carbon (Cable et al., 2014; Garnello et al., 2021) into the atmosphere (Bowden, 2010; Biskaborn et al., 2019; Smith et al., 2022). Permafrost thaw and thermokarst processes make these boreal forests extremely vulnerable to climate warming scenarios (Soja et al., 2007; Farquharson et al., 2019; Zandt et al., 2020; Garnello et al., 2021). Trees growing in these regions are highly sensitive to climate change and record summer air temperature signals well (Vaganov et al., 2006). However, starting from 1990s a reduced sensitivity of tree growth to summer air temperature was reported at some boreal sites in the American and Canadian subarctic (Briffa et al., 1998), potentially linked to warming-induced drought stress (Wilmking et al., 2004; D'Arrigo et al., 2008; Porter and Pisaric, 2011; Porter et al., 2013). The emergence of this decoupling and the need for long-term hydroclimatic information has stimulated the search for alternative tree-ring climate proxies in affected regions. Stable carbon and oxygen isotopes ($\delta^{13}C_{trc}$, $\delta^{18}O_{trc}$) in tree rings were proven as useful proxies for temperature and precipitation changes (Roden et al., 2000; McCarroll and Loader, 2004; Porter et al., 2009; Churakova (Sidorova) et al., 2022; Siegwolf et al., 2022). The use of hydrogen isotopes (δ^2H) in precipitation samples have been studied at a global scale and broadly correlate with mean global temperature (Dansgaard, 1964; Konecky et al., 2020). However, only few studies have examined the potential use δ^2H in tree rings as a paleoenvironmental proxy (Roden et al., 2000; Hilasvuori, 2011; Voelker et al., 2014; Kimak and Leuenberger, 2015; Arosio et al., 2021; Lehmann et al., 2021; Schuler et al., 2022; Churakova Sidorova et al., 2022a). Recent studies showed that δ^2H in tree-ring cellulose (δ^2H_{trc}) is more than a temperature proxy and can contain information about biochemical processes related to photosynthesis and ecohydrological changes (Lehmann et al., 2021; Schuler et al., 2022).

In this study, we aim to (i) develop annually resolved stable isotope chronologies of spruce tree-ring cellulose ($\delta^{13}C_{trc}$, $\delta^{18}O_{trc}$, δ^2H_{trc}) from the western Canadian subarctic (CAN), an area where decoupling between modern air temperature and tree growth has been observed and test these triple isotope proxies as indicators for temperature, moisture and solar irradiation changes over the past century; (ii) perform comprehensive climate analyses of newly obtained and previously published centennial stable isotope chronologies from six tree species and from 24 research sites located at high-latitudinal (HL) and - altitudinal (HA) as well as Siberian (SIB) transects in the Northern Hemispheric boreal zone to assess driving climatic factors; and (iii) assess the suitability of triple isotopes in conifers' tree-ring cellulose for the application to paleoclimatic reconstructions.

2. Material and methods

2.1. Boreal climate characteristics

The boreal forest broadly overlaps with the circumpolar permafrost zone (Helbig et al., 2017), including regions that are underlain by limited to no permafrost (e.g., southern Canada and western Europe) and more northern regions of the Canadian and Siberian Arctic where permafrost distribution is more continuous (Fig. 1a).

Boreal forest soils vary from podzolic, sod, sod-podzolic, permafrost-taiga, illuvial-humus-iron podzols, podburs and peat (Abaimov et al., 1997). Low temperatures lead to low nutrient availability, which is currently increasing due to warming and higher microbiological activity in the soil. In regions that do contain permafrost, the active layer (AL) that thaws once per year reaches a maximum depth (typically in the late summer or early fall months) of ~40 cm in the colder, more continental areas of the boreal forest, and up to ~100 cm in northern Scandinavia, which lacks permafrost availability. Intra-annual climate variability is high for the subarctic region. Highly continental boreal sites experience an extreme range of air temperature characterized by harsh winters, with daily minimum – 55 °C and annual average temperature – 14 °C in Yakutia and rather short (up to 70–90 days) and hot summers, with daily maximum temperature, which can reach + 45 °C and mean annual air temperature of 1.2 °C in Siberian transect at the southern boreal region in Khakassia (KHAK, Table 1), e.g., Köppen zones Dfc and Dwc, Abaimov et al., 1997; Knorre et al., 2006, Vaganov et al., 2006; Boike et al., 2013; Churakova (Sidorova) et al., 2022a, 2022b. The sum of annual precipitation varies across high-latitudinal sites from 205 mm in eastern part up to 2035 mm /year in the western part of subarctic (Table 1). The low albedo of the boreal forest plays an important role in regulating the surface energy balance and climate of the high-latitudinal subarctic (Bonan, 2008). Sunshine duration and cloud cover are rather variable across boreal regions. In summer, sunshine duration lasts longer at high latitudes than at the southern taiga and forest steppe zone (Young et al., 2012; Gagen et al., 2016; Churakova (Sidorova) et al., 2019, 2022a, 2022b; Churakova-Sidorova et al., 2022).

2.2. Boreal tree species

There are six main conifer tree species, which were considered in this study across the boreal zone: white spruce (*Picea glauca* (Moench) Voss), and black spruce (*Picea mariana* Mill.) in western subarcic in Canada and Alaska; Scots pine (*Pinus sylvestris* L.) in Fennoscandia, and a variety of larch tree species (*Larix sibirica* Ledeb., *Larix gmelinii* (Rupr.) Rupr., *Larix cajanderi* Mayr.) in central, eastern and northeastern Siberia (see Table 1).

Living larch trees growing at the high latitudes in Siberia can reach 878 years (Sidorova et al., 2008). Larch snags (dead stems resting on the surface) have a good preservation in the colder permafrost regions, with some of the oldest dated specimens having lived >1200 years ago (Sidorova et al., 2008). While living larch trees from high-elevated sites, e.g., in the Altai-Sayan Mountain Range (Table 1) can reach 1307 years, which is an absolute record for the boreal zone (Taynik et al., 2023).

2.3. Tree-ring stable isotope chronologies

Annually resolved stable carbon, oxygen and hydrogen isotope chronologies in white spruce tree-ring cellulose ($\delta^{13}C_{trc}$, $\delta^{18}O_{trc}$, and δ^2H_{trc}) based on five tree cores were developed for this study of the western part of the Canadian subarctic (CAN, Table 1). This is the first triple isotope record from the northern Canadian Arctic. Earlier carbon and oxygen isotope chronologies were developed from Quebec taiga with 5-year block resolution (Naulier et al., 2015; Gennaretti et al., 2017) and from the Mackenzie Delta region (Porter et al., 2009, 2014, Porter and Pisaric, 2011, Table 1). There are no δ^2H_{trc} time series were obtained to our knowledge.

Additionally, published $\delta^{13}C_{trc}$, $\delta^{18}O_{trc}$, and δ^2H_{trc} data from 14 sites at HL; 5 sites from SIB and 4 sites from HA transects (Fig. 1a, Table 1) were included in the comparative analysis with CAN. Only 5 of these additional sites, however, have triple isotope datasets. Monthly ERA5 gridded

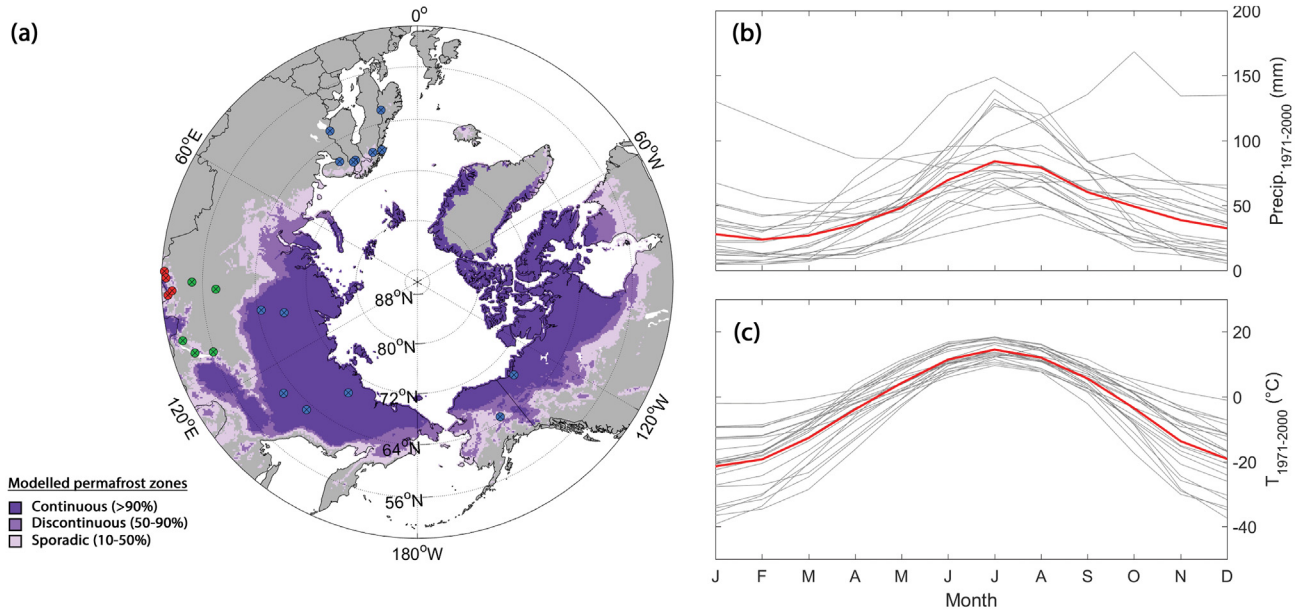

Fig. 1. The location of the study sites with available stable isotopes are grouped from west to east for the subarctic regions along latitudinal transect (HL); for the Siberian transect sites are grouped from taiga to forest-steppe zone and to the Lake Baikal region (SIB); and the Altai-Sayan Mountain Range sites are grouped according to the high-altitudinal transect (HA) (a). Monthly precipitation (b) and temperature (c) distribution for the common period (1971–2000) for all study sites was calculated based on the ERA5 gridded data (Obu et al., 2019; Hersbach et al., 2020). Continuous (> 90 %), discontinuous (50–90 %) and sporadic (10–50 %) modelled permafrost zones are indicated from purple (> 90 %) to a light rose (10–50 %) colors.

precipitation (Fig. 1b) vary significantly from region to region, contrary to the rather homogeneous distribution of monthly ERA5 gridded (Obu et al., 2019; Hersbach et al., 2020) air temperature data (Fig. 1c) during the common period of climate observation 1961–2000.

2.4. Stable carbon, oxygen and hydrogen isotope analyses

For the CAN site (Table 1), annual tree rings from five tree cores of *Picea glauca* were split manually using scalpel under the binocular (Leica, Carl Zeiss, Germany). Stable hydrogen oxygen and carbon, isotope analyses for the period 1900–2009 were conducted. Each wood subsample for each year was enclosed individually in a filter bag (F57, Ankom Technology, NY, USA) and washed twice for 2 h in 5 % NaOH to remove lipids, resins and hemicellulose. A 7 % $NaClO_2$ treatment was then performed for 36 h to remove the lignin (see Loader et al., 1997). Samples were washed and dried in the oven for 24 h at 50 °C, then homogenized using ultrasound and freeze-dried under vacuum. Each extracted tree-ring cellulose sample was weighed (ca. 1.0 mg) and packed into silver or tin capsules for isotope analysis.

For hydrogen isotope analysis, it is necessary to exclude the effect of exchangeable hydrogen. Two approaches are available: a) nitration of cellulose or b) equilibration of the cellulose with water of known isotopic composition, followed by correction procedure to obtain the δ^2H of carbon-bound hydrogen. In this paper, we followed the second approach, based on a new protocol as described in detail in Schuler et al. (2022). Briefly, the samples are equilibrated with hot water vapor (130 °C) in a closed chamber for two hours and then dried with N_2 still in the same chamber at the same temperature. The samples are then transferred to the autosampler of the pyrolysis-device, which is flushed with argon continuously, and then converted by high-temperature conversion at 1420 °C to H_2 with subsequent analysis in the Isotope Ration Mass Spectrometer (IRMS) (MAT 253, Thermo, Germany) (Loader et al., 2015). Samples from previous studies (ISONET) were prepared and analyzed as described in Vitali et al. (2022).

Stable carbon isotope analysis was performed at the stable isotope facility of the Paul Scherrer Institute, Villigen PSI and the Swiss Federal Institute for Forest, Snow and Landscape Research WSL, Switzerland using the same facilities and operational personal.

Cellulose samples (0.2–0.3 mg) for IND, PYAD, TAY, ENE, TUR, KHAK, ALT (Table 1) were weighed into tin capsules for the analysis of the $^{13}C/^{12}C$ using an isotope ratio mass spectrometer delta-S (Finnigan MAT, Bremen, Germany) linked to two elemental analyzers (EA-1110 Carlo Erba, Italy) via a variable open split interface (CONFLO-II, Finnigan MAT, Bremen, Germany). The $^{13}C/^{12}C$ was determined by combustion under excess of oxygen at a reactor temperature of 1020 °C, operating in continuous flow mode at the PSI, Switzerland.

Cellulose samples for the sites at HO, CH and CAN were weighted into the silver capsules (ca. 1 mg) and analyzed with a vario PYRO cube (Elementar, Hanau, Germany) via thermal decomposition at 1450 °C and conversion to CO under O_2 exclusion in helium (Woodley et al., 2012). This system was linked to the IRMS (Delta plus XP, Thermo Finnigan, Bremen, Germany) at the Swiss Federal Institute for Forest, Snow and Landscape Research WSL, Switzerland. During pyrolysis of cellulose a small (but constant) amount of carbon is added to the resulting CO, which is used for isotope analysis of both carbon and oxygen. Extensive tests were done to establish a correction function for this effect by analysis of a sub-set of samples on both instruments ($\delta^{13}C_{corrected} = 1.1142 \cdot \delta^{13}C_{raw} + 1.45$) (Weigt et al., 2015) as well as analysis of internal reference materials of known isotopic composition with each sequence to verify this correction. The same facilities and method were used for data obtained within European ISONET project by Vitali et al. (2022) for the Scandinavian sites GUT, INA, and ILO; and within MILLENNIUM project for the sites: FOR, TOR, LAN, and KOL (Table 1).

An interlaboratory comparison among 9 European research laboratories reported by Boettger et al. (2007) showed a good agreement between results within the precision of the isotope ratio mass spectrometry (IRMS) method used: (0.2 ‰ for carbon and 0.3 ‰ for oxygen).

Both systems the EA-IRMS and the PYRO cube yielded very similar precisions (± 0.2 ‰) and the values from the two instruments were in high agreements (better than the measurement precisions) (Weigt et al., 2015). The precision (± 0.1 ‰ for $\delta^{13}C$, ± 0.3 ‰ for $\delta^{18}O$ and ± 2 ‰ for δ^2H)

Table 1
Newly developed and available tree-ring stable carbon ($\delta^{13}C_{trc}$), oxygen ($\delta^{18}O_{trc}$) and hydrogen ($\delta^{2}H_{trc}$) isotope chronologies across boreal zone. Sites are grouped from west to east for the subarctic regions along high-latitudinal transect (HL); for the Siberian transect, sites are grouped from taiga to forest-steppe zone and to the Lake Baikal region (SIB); and for the Altai-Sayan Mountain Range sites are grouped according to the high-altitudinal transect (HA). Data sets are not available are indicated as (NA). Annual air temperature and precipitation are calculated for the common period from 1971 to 2000 from the local weather station data (meteo.ru; climate.weather.gc.ca and https://climexp.knmi.nl). Stable isotopes in precipitation are available on the Online Isotopes in Precipitation Calculator (waterisotopes.org; Bowen and Revenaugh, 2003). Access status 24 April 2022.

Site name, code	Site coordinates, elevation (m asl)	Weather station, coordinates, elevation (m asl)	Tree species	Stable isotopes in tree-ring cellulose, study period			Stable isotopes in precipitation waterisotopes.org		Annual temperature °C	Precipitation mm/year	References and Target dataset URL
				$\delta^{13}C_{trc}$	$\delta^{18}O_{trc}$	$\delta^{2}H_{trc}$	$\delta^{18}O_{w}$	$\delta^{2}H_{w}$			
High latitudes (HL)											
Central Alaska ALA	64° 42′ N, 148° 18′ W (290 m asl)	Bonanza Creek 64° N, 148° W (116 m asl) climate.weather.gc.ca	*P. glauca*	1800–1996	NA	NA	1985–1987 2002–2021	1985–1987 2002–2021	−3.4	312	Barber et al., 2000
Mackenzie Delta MZ	68° 24′ N, 133° 49′ W (3 m asl)	Inuvik 68° N, 133° W (15 m asl) climate.weather.gc.ca	*P. glauca*	1850–2003	1780–2003	NA	2013–2018	2013–2018	−9.6	245	Porter et al., 2009, 2014, Porter and Pisaric, 2011
Western Canada CAN	68° 24' N, 133° 49' W (3 m asl)	Inuvik 68° N, 133°W (15 m asl) climate.weather.gc.ca	*P. glauca*	*1990–2009	*1990–2009	*1900–2009	2013–2018	2013–2018	−9.6	245	*This study
Gutulia GUT	62° N, 12° E (800 m asl)	Gutulia 62° N, 12′ E (800 m asl) Isonet climate data, Vitali et al., 2022	*P. sylvestris* L.	1905–2002	1905–2002	1905–2002	2004–2019	2004–2019	0.8	2035	Vitali et al., 2022
Forfjord, Vesterålen FOR	68° 48′ N, 15° 44′ E (10–100 m asl)	Tromso 69° N, 18° E, (10 m asl) climate.weather.gc.ca	*P. sylvestris* L.	990–2001	NA	NA	2018–2020	2018–2020	2.4	1353	Young et al., 2012 https://doi.org/10.25921/zvgf-n290
Torneträsk TOR	68° N, 19° E (450 m asl)	Abisko 68° N, 18°E (385 m asl) climate.weather.gc.ca	*P. sylvestris* L.	900–2008	NA	NA			−1.8	670	Loader et al., 2013 https://doi.org/10.25921/m9se-1691
Laanila LAN	68° N, 27° E (220 m asl)	Sodankylä, 67° N, 26° E (179 m asl) https://www.ilmatieteenlaitos.fi/	*P. sylvestris* L.	800–2002	NA	NA	2019–2020	2019–2020	−2.3	460	Gagen et al., 2012
Kessi Inari INA	68° 9′ N, 28° 4′ E (150 m asl)	Kessi Inari 68° N, 28° E (150 m asl) Isonet climate data, Vitali et al., 2022	*P. sylvestris* L.	1905–2002	1905–2002	1905–2002	2019–2020	2019–2020	−1.6	452	Vitali et al., 2022
Ilomantsi ILO	62° 9′ N, 30° 9′ E (200 m asl)	Ilomantsi 62° N, 31° E (200 m asl) Isonet climate data, Vitali et al., 2022	*P. sylvestris* L.	1905–2002	1905–2002	1905–2002	2000–2007	2000–2007	1.6	637	Vitali et al., 2022
Khibini, Kola Peninsula KOL	67° N, 33° E (761 m asl)	Khibini 67° N, 33° E (761 m asl) meteo.ru	*P. sylvestris* L.	1900–2000	NA	NA	NA	NA	−1.8	606	Kononov et al., 2009
Taimyr Peninsula TAY	68° N, 103° E (300 m asl)	Khatanga 71° N, 102° E (33 m asl) meteo.ru	*L. gmelinii* Rupr. Rupr.	516–2020	516–2020	1900–2020	2007–2009	2007–2009	−13.2	269	Sidorova et al., 2013a Churakova (Sidorova) et al., 2021a, 2022a, 2022b https://doi.org/10.5281/zenodo.6635877

Spasskaya Pad PYAD	62° 14′ N, 129° 37′ E (220 m asl)	Spasskaya Pad, 62° N, 130° E (220 m asl)	*P. sylvestris* L.	1780–2008	1901–2013	NA	NA	NA	−10	233	Timofeeva, 2017
Suntar Khayata Yakutia YAK	63° N, 139° E (900 m asl)	Chokurdakh 70° N, 147° E (11 m asl) meteo.ru	*L. cajanderi* Mayr	1599–2000	NA	NA	1996–2000	1996–2000	−12.3	334	Kirdyanov et al., 2008
Indigirka IND	69° N, 148° E (350 m asl)	Chokurdakh 70° N, 147° E (11 m asl) meteo.ru	*L. cajanderi* *Mayr*	516–2021	516–2021	1900–2021	NA	NA	−14.7	205	Churakova (Sidorova) et al., 2020, 2022a, 2022b; Sidorova et al., 2008, 2011 https://doi.org/10.48620/4 https://doi.org/10.5281/zenodo.6635877
Tura TUR	64° 32′ N, 100° 14′ E (168 m asl)	Tura 64° N, 100° E (168 m asl) meteo.ru	*L. gmelinii* Rupr. Rupr.	1864–2006	1864–2006	NA	NA	NA	−9.1	368	Sidorova et al., 2009
Siberian transect (SIB)											
Eniseysk ENE	58° N, 92° E (150 m asl)	Eniseysk 58° N, 92° 19 E (150 m asl) meteo.ru	*L. sibirica* Mayr.	1850–2000	1850–2000	NA	2014–2016	2014–2016	−1.8	474	Knorre et al., 2023 in preparation
Khakasia KHAK	54° 24’ N, 89° 57′ E (477 m asl)	Minusinsk 53° N, 91° E (250 m asl) meteo.ru	*L. sibirica* Ledeb.	1850–2005	1850–2005	NA	2014–2016	2014–2016	1.2	300	Knorre et al., 2010
Irkutsk IRK	52° N, 104° E (530 m asl)	Irkutsk 52° N, 104° E (46 m asl) meteo.ru	*L. sibirica* Ledeb.	1734–1998	1734–1998	NA	2011–2019	2011–2019	0.1	503	Tartakovsky et al., 2012 https://doi.org/10.25921/3mjn-9827
Olkhon Island Baikal Lake region OLH	53° 17′ N, 107° 38′ E (530 m asl)	Irkutsk 52° N, 104° E (46 m asl) meteo.ru	*L. sibirica* Ledeb	1952–1998	1952–1998	NA	NA	NA	−2.5	376	Tartakovsky et al., 2012 https://doi.org/10.25921/3mjn-9827
Davan Pass DAV	55° 51′ N, 108° 55′ °E (1400 m asl)	Irkutsk 52° N, 104° E, (46 m asl) meteo.ru	*L. sibirica* Ledeb	1388–2000	1388–2000	NA	1996–2000	1996–2000	−8.2	473	Tartakovsky et al., 2012 https://doi.org/10.25921/3mjn-9827
High altitudes (HA)											
Altai AL	50° 24′ N, 87° 33′ E (2300 m asl)	Barnaul 53° N, 83° E (189 m asl) meteo.ru	*P. sibirica* Du tour	1954–2000	1954–2000	NA	2014–2015	2014–2015	−4.3	461	Loader et al., 2010
Altai ALT	50° 38′ N, 89° 06′ E (2280–2400 m asl)	Mugur-Aksy 50° N, 90° E (1823 m asl) meteo.ru	*L. sibirica* Ledeb	516–2016	516–2016	NA	NA	NA	−4.9	328	Sidorova et al., 2012, 2013b; Churakova (Sidorova) et al., 2019; Churakova-Sidorova et al., 2022 https://doi.org/10.5281/zenodo.6467290
Ersin Tyva Republic HO	50° 50′ N, 93° 01′ E (1502 m asl)	Ersin 50° N, 95° E (1104 m asl) meteo.ru	*L. sibirica* Ldb.	1919–2019	1919–2019	NA	2012	2012	−3.7	197	Churakova (Sidorova) et al., 2021a; Churakova-Sidorova et al., 2022
Chadan Tyva Republic CH	51° 28′ N, 91° 58′ E (832 m asl)	Chadan 51° N, 91° E (817 m asl) meteo.ru	*L. sibirica* Ldb.	1919–2019	1919–2019	NA	NA	NA	−2.1	301	Churakova (Sidorova) et al., 2021a; Churakova-Sidorova et al., 2022

is based on a large number of measurements of the standard material international reference standards ($n = 99$).

The isotopic ratios are expressed in the conventional delta notation (δ) expressed in (‰) relative to the international standards (Eq. (1)):

$$\delta_{sample} = \left(R_{sample}/R_{standard}-1\right) \bullet 1000, \quad (1)$$

where R_{sample} is the ratio of $^{13}C/^{12}C$ or $^{18}O/^{16}O$ or $^{2}H/^{1}H$ in the sample and $R_{standard}$ is the ratio either for carbon ($^{13}C/^{12}C$) in the Vienna Pee Dee Belemnite (VPDB) or for oxygen ($^{18}O/^{16}O$) and hydrogen ($^{2}H/^{1}H$) in the Vienna Standard Mean Ocean Water (VSMOW).

The correction for changing $\delta^{13}C$ of atmospheric CO_2 (Francey et al., 1999) was applied for all chronologies considered in this study as well as for newly developed $\delta^{13}C_{trc}$ from CAN for the period from 1900 to 2009. While no specific corrections for the $\delta^{18}O$ and $\delta^{2}H$ were applied.

2.5. Estimation of precipitation isotopes

Long-term monthly and annual averages of $\delta^{2}H$ and $\delta^{18}O$ in precipitation ($\delta^{2}H_{prec}$ and $\delta^{18}O_{prec}$) were calculated for all sites based on the coordinates, elevation, country, and collection date using the online isotopes in precipitation calculator (waterisotopes.org; Bowen and Revenaugh, 2003). For subarctic Siberian sites, however, data for precipitation are scarcely represented and available data sets are relatively short and limited to the last 20 years (Table 1).

2.6. Climate data

Climatic data recorded at the local weather stations are limited to the length starting for all study sites from 1971 to 2000 compared to the gridded large-scale climate data (CRU TS v.4, 0.5° latitude by 0.5° latitude grid, http://climexp.knmi.nl) (Harris et al., 2020) from 1901 to 2000. However, almost 40 % of precipitation, vapor pressure deficit, relative humidity and sunshine duration data are not well represented by gridded data for the Siberian and Canadian regions from 1901 to 1950 (Zharkov et al., 2021). Yet, these moisture and sunshine duration parameters are more accurately recorded by local weather stations (Zharkov et al., 2021). Despite that the air temperature gridded data significantly correlated with the local weather stations for all studied sites (> 0.90–0.93, $P < 0.01$) for the period from 1901 to 2000, to be consistent in comparing temperature, precipitation and sunshine duration patterns, we choose the common period 1971–2000 for climate data from local weather stations for all sites (Table 1).

2.7. Statistical analysis

Statistical differences, standard deviations and standard errors were calculated between newly obtained and used for the comparative analyses time series.

Pearson correlation coefficients (r) and coefficient of determination (R^2) were calculated between newly developed and available stable tree-ring isotope chronologies across the boreal zone (6 research sites for $\delta^{2}H_{trc}$; 24 sites for $\delta^{13}C_{trc}$ and 18 sites for $\delta^{18}O_{trc}$) versus publicly available climate data obtained from the local weather stations (Table 1) over the common period (1971–2000) of instrumental observations. Statistical nonparametric Mann–Whitney test for randomly selected medians was applied. The code for climate data analysis with triple stable isotopes $\delta^{13}C_{trc}$, $\delta^{18}O_{trc}$, $\delta^{2}H_{trc}$ is available via GitHub link https://github.com/mikewellmeansme/trs-isotopes-analyser

Heat maps were generated using Seaborn (Python package for data visualization) (Waskom, 2021).

We used all six $\delta^{2}H_{trc}$ time series from 1901 to 2000 to perform a principal components analysis (PCA). For that we normalised each time series by calculating anomalies and standard deviation with respect to the full period. We also linearly detrended the normalised time series to focus on inter-annual climate variability and to avoid extracting a trend signal in the PCA, but the detrended and non-detrended time series are effectively identical. We refrained from performing more sophisticated detrending as we did not find an argument for doing so. Then we extracted the time series for the two leading principal components, where the first principal component explains 21 % and the second principal component explains 19 % of the variance in the data set.

For the correlation analysis with atmospheric circulation patterns, we use the National Oceanic and Atmospheric Administration 20th Century Reanalysis Version 3 (20CRv3) (Slivinski et al., 2019). The ensemble mean of 80 members was used over the period from 1901 to 2000. The 20CRv3 was found to represent global climate variability very well, with substantial improvements over previous versions (Slivinksi, 2021).

3. Results

3.1. Statistical characteristics of stable isotope chronologies

3.1.1. Assessment of mean, median, minimum and maximum values

Median $\delta^{2}H_{trc}$ value from newly developed CAN chronology over the period from 1900 to 2009 showed (- 146 ‰) compared to more depleted value in northeastern subarctic IND (- 172 ‰) site. Mann–Whitney test for randomly selected medians showed significant differences between values at the $P < 0.0000$ (Fig. 2a). Higher values observed for the Scandinavian subarctic ranging within - 94 to - 105 ‰ which are significantly differ from the western and eastern HL sites ($P < 0.0000$).

A relatively high standard deviation (SD) calculated over the period from 1900 to 2009 was revealed for $\delta^{2}H_{trc}$ from IND ($\sigma = 10.9$ ‰) compared to other sites (Fig. 2a). Annually resolved $\delta^{18}O_{trc}$ (Fig. 2b) showed clear isotopic differences along HL transect from the cold western sites in the Canadian subarctic and northeastern subarctic (19 ‰ for CAN and IND) to the warmest sites in the Scandinavian subarctic (up to 27.6 ‰ for GUT). The $\delta^{18}O$ data obtained from the forest-steppe zone in SIB transect for KHAK and HA transect in the Altai-Sayan Mountain Range show similarly high values (26.4 ‰) and (27.7 ‰) for both sites, respectively (Fig. 2b).

The mean $\delta^{13}C_{trc}$ values along HL transect from west to east vary only in a moderate range between −22.6 to −24 ‰ (Fig. 2c, *blue color*). Higher standard deviation was found for the site from Norway, FOR (SD = 0.8) compared to $\delta^{13}C_{trc}$ from northeastern IND (SD = 0.6).

The $\delta^{13}C_{trc}$ across SIB transect vary significantly ($P < 0.0000$) from taiga zone site in ENE (-22.24 ‰) and the Lake Baikal region (-22.01 ‰) to the forest-steppe zone in KHAK (- 20.3 ‰) (Fig. 2c, *green color*). The HO and CH sites from HA transect in the Altai-Sayan Mountain Range shows median value (-21.3 ‰) calculated over the period from 1919 to 2009 showing statistically significant difference ($P < 0.0000$) with SIB and northeastern part of HL transects, except of western part of subarctic HL.

3.1.2. Comparison of water isotopes and temperature with tree-ring isotopes

Water isotopes in precipitation ($\delta^{18}O_{prec}$ and $\delta^{2}H_{prec}$) calculated from the limited number of available stations (Bowen and Revenaugh, 2003) shows a significant regression close to the Global Meteoric Water Line (GMWL) (Table 1, Fig. 3a). Only few $\delta^{18}O_{trc}$ and $\delta^{2}H_{trc}$ chronologies from IND, TAY, CAN, INO, ILA, GUT are available for the regression analysis (Fig. 3b).

Significant regressions were found between the water isotopes in precipitation $r = 0.99$, $P < 0.001$; $\delta^{2}H_{prec} = 8.95 + 8.30 \bullet \delta^{18}O_{prec}$ (Fig. 3a) and in tree-ring cellulose $r = 0.96$, $P < 0.002$; $\delta^{2}H_{trc} = -312.7 + 7.90 \bullet \delta^{18}O_{trc}$ (Fig. 3b). Positive significant regression coefficients were found between annual temperature versus $\delta^{18}O_{prec}$ $r = 0.58$, $P < 0.05$; $\delta^{18}O = -12.18 + 0.61 \bullet T_{annual}$ (Fig. 3c) and annual temperature versus $\delta^{2}H_{prec}$ $r = 0.59$, $P < 0.05$; $\delta^{2}H = -92.04 + 5.15 \bullet T_{annual}$ (Fig. 3d). Positive significant regressions were revealed between local weather stations data (Table 1) versus available and newly developed $\delta^{18}O_{trc}$ ($r = 0.62$, $P < 0.001$, $\delta^{18}O_{trc} = 26.1 + 0.44 \bullet T_{annual}$, Fig. 3e) and $\delta^{2}H_{trc}$ (r = 0.96, $P < 0.001$, $\delta^{2}H_{trc} = -100.7 + 4.39 \bullet T_{annual}$, Fig. 3f).

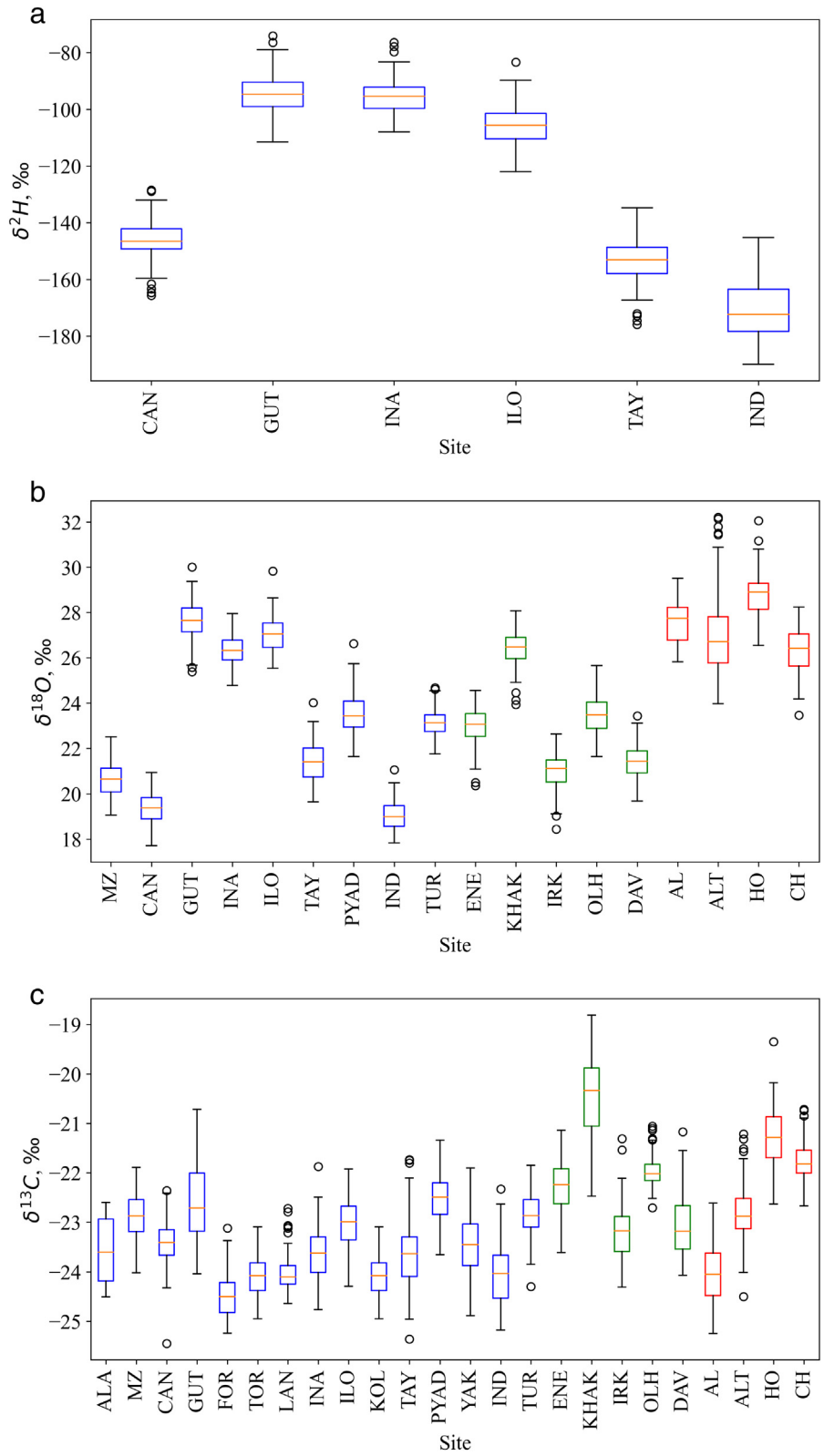

Fig. 2. Box plot of multiple variables: median, 25–75 %, Whisker non-outlier range (maximum and minimum) for stable isotopes in tree-ring cellulose (a) δ^2H_{trc}, (b) $\delta^{18}O_{trc}$ and (c) $\delta^{13}C_{trc}$ across high-latitudinal transect from west to east (HL, *blue color*); Siberian transect, where sites are grouped from taiga to forest-steppe zone and to the Lake Baikal region (SIB, green color); and for the Altai-Sayan Mountain Range, where sites are grouped according to the altitudinal transect (HA, red color). The names for the abbreviations of the sites are listed in Table 1.

Two temperature-depended groups along HL transect were revealed based on the δ^2H_{trc} (Fig. 3f). The first group is defined by an extremely cold environment in the permafrost zone and low temperatures (CAN, TAY and IND) and the second one (GUT, INA, ILO) from the Scandinavian subarctic, which is not covered by permafrost and affected by warmer temperatures and larger amount of precipitation (Table 1).

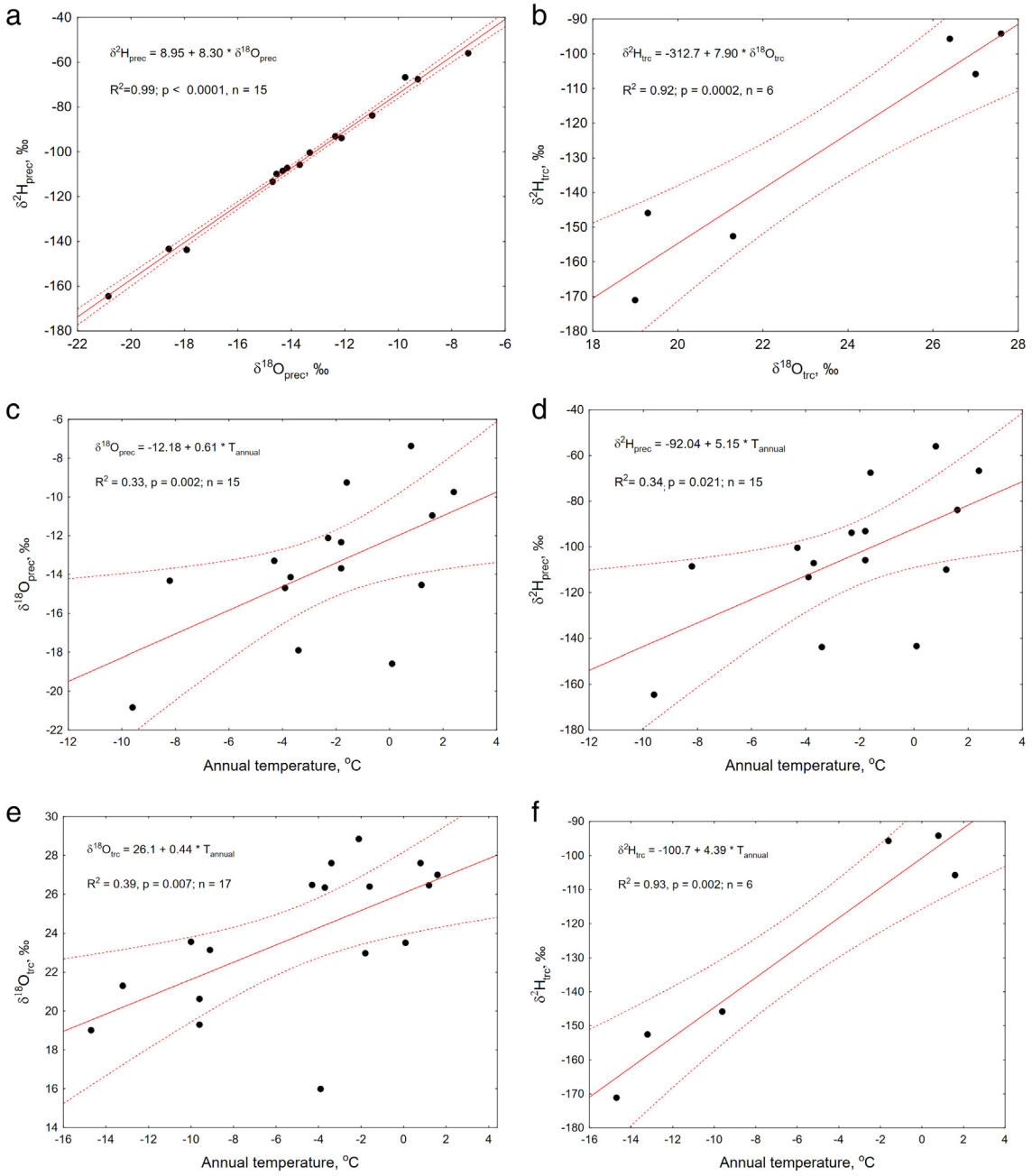

Fig. 3. Regression line of δ^2H_{prec} versus $\delta^{18}O_{prec}$ (a) in precipitation from available weather stations data (Table 1). HL-sites: ALA, CAN, LAN, FOR, GUT, ILO, INA; SIB-sites: ENE, KHAK, IRK, DAV; and HA-sites: AL and HO, ALT (waterisotopes.org, Bowen and Revenaugh, 2003) and (b) newly developed δ^2H_{trc} versus $\delta^{18}O_{trc}$ in tree-ring cellulose. The names for the abbreviations of the sites are listed in Table 1. Annual temperature obtained from the local weather stations (Table 1) versus available $\delta^{18}O_{prec}$ (c) and δ^2H_{prec} (d) as well as versus newly developed and available $\delta^{18}O_{trc}$ (e) and δ^2H_{trc} (f) data, correspondingly. Confidential Interval is marked at 0.95.

3.2. Centennial variability and trends

3.2.1. Trend analysis

Concerning hydrogen isotope chronologies, δ^2H_{trc}-TAY shows a significant ($R^2 = 0.38$; $P < 0.0000$) decreasing trend in the last 20 years, in contrast to other sites (Fig. 4a). Normalised relative to the zero (z-score) δ^2H_{trc}-CAN chronology shows a relatively stable trend ($R^2 = 0.38$; $P < 0.0000$) towards the 2000s, while an abrupt decrease was found in the 1900s. The tree-ring δ^2H_{trc}-IND shows a significant trend ($R^2 = 0.43$; $P < 0.0000$) with a clearly higher variability compared to other HL sites and an apparent step-change (nearly ~20 ‰ decrease) that occurred in the 1950s. A slight decline around the 1950s is observed for Finish ILO site ($R^2 = 0.27$; $P < 0.001$) (Fig. 4a). While increasing trends over the last few decades, along with the δ^2H_{trc}-IND chronology were recorded for δ^2H_{trc}-INA ($R^2 = 0.30$; $P < 0.0001$) and ILO sites.

Trends towards the 2000s are significantly increased for $\delta^{18}O_{trc}$ from CAN ($R^2 = 0.17$; $P < 0.0001$), TAY ($R^2 = 0.32$; $P < 0.0000$) and IND ($R^2 = 0.15$; $P < 0.00003$). While trends were significantly declined for the Scandinavian site INA ($R^2 = 0.42$; $P < 0.000$ (Fig. 4b).

For $\delta^{13}C_{trc}$, increasing trends were revealed mainly for the Scandinavian sites (e.g., INA $R^2 = 0.57$; $P < 0.0000$; ILO $R^2 = 0.58$; $P < 0.0000$ and GUT $R^2 = 0.62$; $P < 0.0000$), while decreasing trends for CAN ($R^2 = 0.35$; $P < 0.000$); TAY ($R^2 = 0.31$; $P < 0.0000$) and IND ($R^2 = 0.20$; $P < 0.0001$) were found (Fig. 4c).

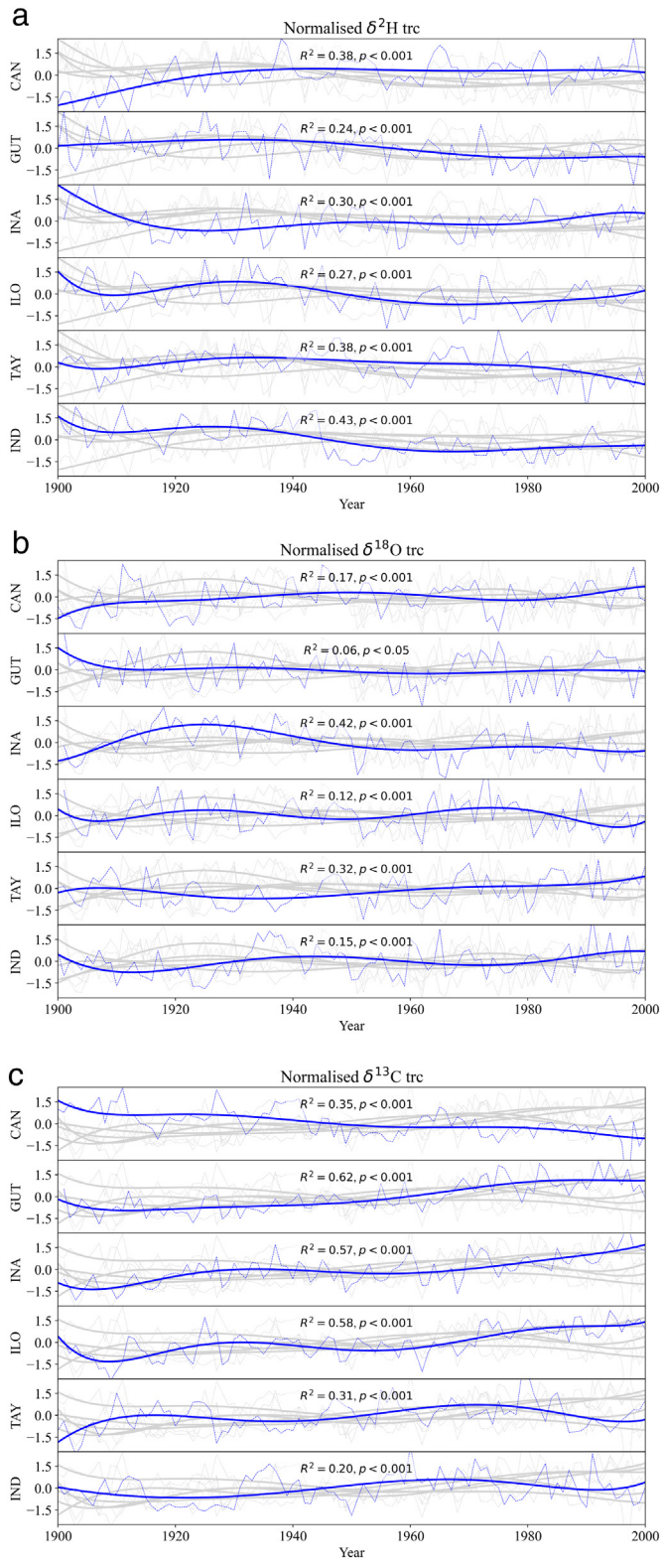

Fig. 4. Normalised relative to the zero (z-scored) (a) δ^2H_{trc}, (b) $\delta^{18}O_{trc}$ and (c) $\delta^{13}C_{trc}$ chronologies from the HL sites (see Table 1). Least squares polynomial fit of degree 6 (*bold blue line*) is applied to all chronologies for the common period for all chronologies 1901–2000. The names for the abbreviations of the sites are listed in Table 1.

3.2.2. Correlation analysis between centennial chronologies

A correlation analysis between δ^2H_{trc}, $\delta^{18}O_{trc}$ and $\delta^{13}C_{trc}$ chronologies was performed ($P < 0.05$) for the common period from 1901 to 2000 for all newly obtained and available chronologies. Negative correlations were revealed between δ^2H_{trc} from HL sites: CAN and IND ($r = -0.31$) as well as between TAY and Scandinavian INA ($r = -0.19$). A positive and significant correlation between the δ^2H_{trc} -IND with ILO chronologies was found ($r = 0.33$) as well as between δ^2H_{trc} GUT and ILO ($r = 0.41$). The $\delta^{18}O_{trc}$ from TAY showed a positive significant correlation with GUT ($r = 0.53$). Positive significant correlations were found between $\delta^{18}O_{trc}$ from GUT and ILO ($r = 0.32$) and INA versus ILO ($r = 0.40$). There are no significant correlations between $\delta^{18}O_{trc}$ from SIB transect and CAN sites. While we found significant correlation between HL and HA transects, specifically between HO and subarctic sites in TAY and IND ($r = -0.61$ and $r = 0.60$), respectively.

Significant correlations were found mainly between $\delta^{13}C_{trc}$ chronologies. Positive significant correlations were found between $\delta^{13}C_{trc}$ from IND and GUT ($r = 0.27$); between all Scandinavian chronologies (GUT, INO, ILO $r = 0.54$–0.71). While negative correlations were detected between $\delta^{13}C_{trc}$ from CAN and TAY sites ($r = -0.36$) as well as ILO ($r = -0.57$) and INA ($r = -0.56$).

3.3. Climate correlations

3.3.1. Air temperature

A positive summer JJA air temperature signal is strongly (r = 0.5–0.6; $P < 0.001$) captured by both $\delta^{13}C_{trc}$ and $\delta^{18}O_{trc}$ chronologies, in particular for HL subarctic sites (Fig. 5a). The δ^2H_{trc} from CAN showed a positive correlation with July air temperature only. Summer air temperature (JJA) signal (Fig. 5a) was significantly recorded in $\delta^{13}C_{trc}$ for 8 out of 24 sites. The highest significant ($P < 0.01$) correlation in July was observed along the HL transect for the Scandinavian LAN ($r = 0.68$), INA site ($r = 0.57$) and for IND ($r = 0.64$) sites with July air temperature.

The summer air temperature signal is positively recoded in $\delta^{13}C_{trc}$ and δ^2H_{trc} from CAN. The $\delta^{13}C_{trc}$ isotope chronologies from the Scandinavian sites (Fig. 5b) show high correlation with summer temperature as well. While $\delta^{13}C_{trc}$-YAK shows a positive, but moderate correlation with July air temperature only.

December air temperatures are captured by both western and eastern sites at HL transect, e.g., $\delta^{18}O_{trc}$ and δ^2H_{trc} from Scandinavian and TAY, IND sites. Positive significant correlations were revealed for $\delta^{18}O_{trc}$ from TAY and δ^2H_{trc} from GUT, and in opposite, negative correlation with δ^2H_{trc} from INA.

Impacts of March and April air temperature on δ^2H_{trc} from Scandinavian (ILO, GUT), northern and northeastern subarctic IND, TAY sites were revealed (Fig. 5a).

Autumn air temperature of the previous year plays a significant role for $\delta^{13}C_{trc}$ from Scandinavian sites showing negative significant correlations. Yet, the $\delta^{18}O_{trc}$ from the HA (ALT) site recorded autumn signal positively (Fig. 5a).

3.3.2. Sunshine duration

Positive significant correlations were revealed between July sunshine duration and stable carbon isotopes obtained for 6 out of 13 sites. The highest significant correlations were found during summer for the northeastern part of the HL transect, e.g., for $\delta^{13}C_{trc}$ and $\delta^{18}O_{trc}$ from IND ($r = 0.54$ and $r = 0.73$; $P < 0.001$), respectively (Fig. 5b).

The $\delta^{13}C_{trc}$ from SIB transect (KHAK) showed a positive correlation with sunshine duration of October of the previous year ($r = 0.52$, $P < 0.01$). Negative significant correlations were found between available sunshine duration during autumn of the previous year and winter of the current year for the HL δ^2H_{trc}- TAY and IND sites (Fig. 5b).

3.3.3. Moisture-related proxies

Available monthly averaged precipitation, relative humidity and vapor pressure deficit data were correlated with available isotope chronologies

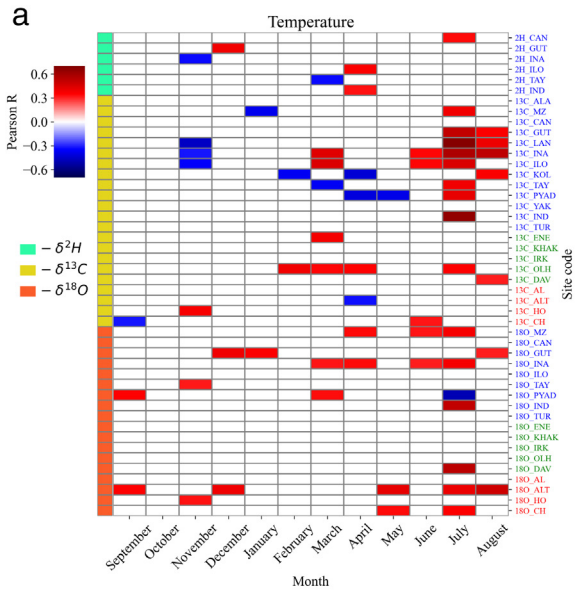
a
Temperature
Pearson R
0.6
0.3
0.0
−0.3
−0.6
$-\delta^2H$
$-\delta^{13}C$
$-\delta^{18}O$
Site code
2H_CAN
2H_GUT
2H_INA
2H_ILO
2H_TAY
2H_IND
13C_ALA
13C_MZ
13C_CAN
13C_GUT
13C_LAN
13C_INA
13C_ILO
13C_KOL
13C_TAY
13C_PYAD
13C_YAK
13C_IND
13C_TUR
13C_ENE
13C_KHAK
13C_IRK
13C_OLH
13C_DAV
13C_AL
13C_ALT
13C_HO
13C_CH
18O_MZ
18O_CAN
18O_GUT
18O_INA
18O_ILO
18O_TAY
18O_PYAD
18O_IND
18O_TUR
18O_ENE
18O_KHAK
18O_IRK
18O_OLH
18O_DAV
18O_AL
18O_ALT
18O_HO
18O_CH
September
October
November
December
January
February
March
April
May
June
July
August
Month

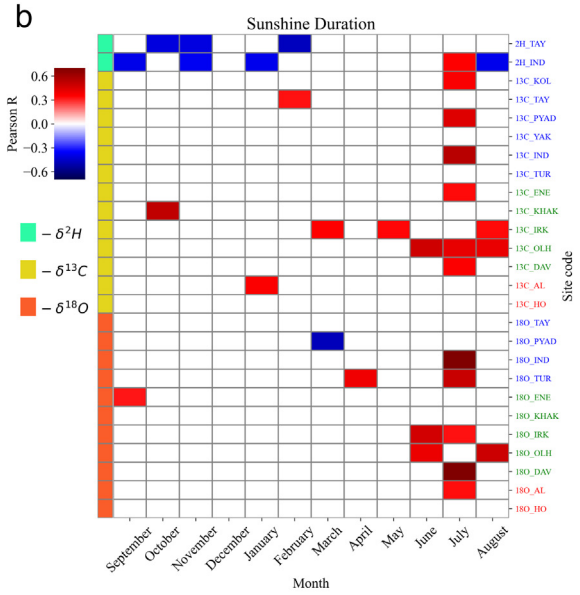
b
Sunshine Duration
Pearson R
0.6
0.3
0.0
−0.3
−0.6
$-\delta^2H$
$-\delta^{13}C$
$-\delta^{18}O$
Site code
2H_TAY
2H_IND
13C_KOL
13C_TAY
13C_PYAD
13C_YAK
13C_IND
13C_TUR
13C_ENE
13C_KHAK
13C_IRK
13C_OLH
13C_DAV
13C_AL
13C_HO
18O_TAY
18O_PYAD
18O_IND
18O_TUR
18O_ENE
18O_KHAK
18O_IRK
18O_OLH
18O_DAV
18O_AL
18O_HO
September
October
November
December
January
February
March
April
May
June
July
August
Month

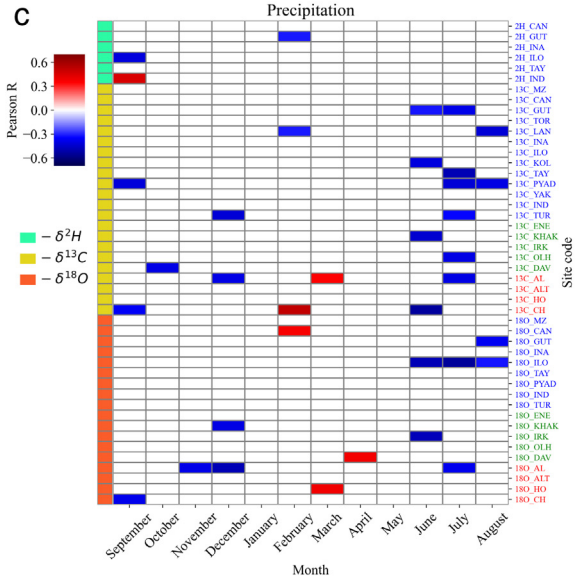
c
Precipitation
Pearson R
0.6
0.3
0.0
−0.3
−0.6
$-\delta^2H$
$-\delta^{13}C$
$-\delta^{18}O$
Site code
2H_CAN
2H_GUT
2H_INA
2H_ILO
2H_TAY
2H_IND
13C_MZ
13C_CAN
13C_GUT
13C_TOR
13C_LAN
13C_INA
13C_ILO
13C_KOL
13C_TAY
13C_PYAD
13C_YAK
13C_IND
13C_TUR
13C_ENE
13C_KHAK
13C_IRK
13C_OLH
13C_DAV
13C_AL
13C_ALT
13C_HO
13C_CH
18O_MZ
18O_CAN
18O_GUT
18O_INA
18O_ILO
18O_TAY
18O_PYAD
18O_IND
18O_TUR
18O_ENE
18O_KHAK
18O_IRK
18O_OLH
18O_DAV
18O_AL
18O_ALT
18O_HO
18O_CH
September
October
November
December
January
February
March
April
May
June
July
August
Month

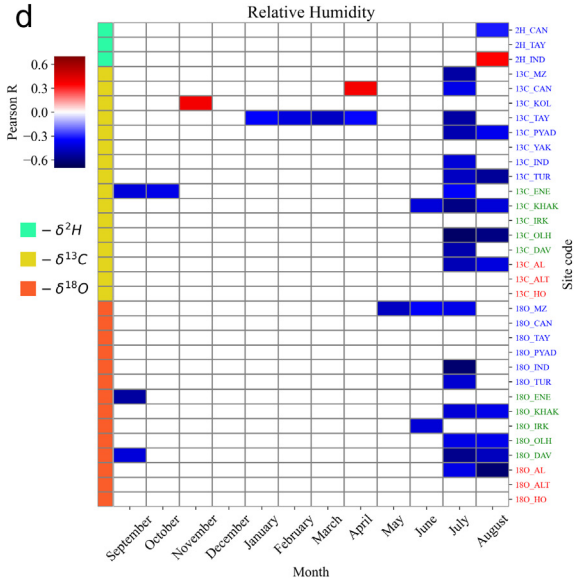
d
Relative Humidity
Pearson R
0.6
0.3
0.0
−0.3
−0.6
$-\delta^2H$
$-\delta^{13}C$
$-\delta^{18}O$
Site code
2H_CAN
2H_TAY
2H_IND
13C_MZ
13C_CAN
13C_KOL
13C_TAY
13C_PYAD
13C_YAK
13C_IND
13C_TUR
13C_ENE
13C_KHAK
13C_IRK
13C_OLH
13C_DAV
13C_AL
13C_ALT
13C_HO
18O_MZ
18O_CAN
18O_TAY
18O_PYAD
18O_IND
18O_TUR
18O_ENE
18O_KHAK
18O_IRK
18O_OLH
18O_DAV
18O_AL
18O_ALT
18O_HO
September
October
November
December
January
February
March
April
May
June
July
August
Month

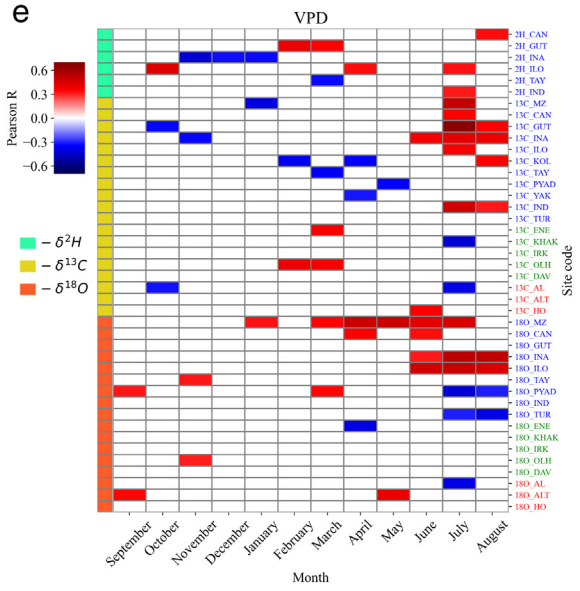
e
VPD
Pearson R
0.6
0.3
0.0
−0.3
−0.6
$-\delta^2H$
$-\delta^{13}C$
$-\delta^{18}O$
Site code
2H_CAN
2H_GUT
2H_INA
2H_ILO
2H_TAY
2H_IND
13C_MZ
13C_CAN
13C_GUT
13C_INA
13C_ILO
13C_KOL
13C_TAY
13C_PYAD
13C_YAK
13C_IND
13C_TUR
13C_ENE
13C_KHAK
13C_IRK
13C_OLH
13C_DAV
13C_AL
13C_ALT
13C_HO
18O_MZ
18O_CAN
18O_GUT
18O_INA
18O_ILO
18O_TAY
18O_PYAD
18O_IND
18O_TUR
18O_ENE
18O_KHAK
18O_IRK
18O_OLH
18O_DAV
18O_AL
18O_ALT
18O_HO
September
October
November
December
January
February
March
April
May
June
July
August
Month

and show a consistent signal for the whole boreal zone (Table 1, Fig. 5c-e). Summer JJA precipitation (Fig. 5c) and relative humidity (Fig. 5d) showed negative significant correlations with carbon and oxygen isotopes mainly for the HL transect, while positive correlations with vapor pressure deficit (VPD) were found for HA sites (Fig. 5e).

There is no significant impact of summer precipitation on hydrogen isotope variability for study sites (6 out of 6) (Fig. 5c). However, negative correlations were obtained between precipitation from autumn of the previous year and with VPD of winter months for the Scandinavian sites only. A positive impact of spring precipitation was found with carbon and oxygen isotopes from HA sites.

Summer VPD is positively and significantly recorded by $\delta^{18}O_{trc}$ from western Canada continuously through spring-summer months (Fig. 5d), while negatively with relative humidity (Fig. 5e).

3.4. Spatial patterns

3.4.1. Spatial winter climate variability recorded in δ^2H_{trc}

Here we correlate each individual time series in the 360 × 180 grids with the PC1 time series. Winter relative humidity shows positive significant correlations ($r \geq 0.3$; $P < 0.01$) with δ^2H_{trc} from central and northeastern part of the HL transect, opposite to negative correlations with δ^2H_{trc} from the western part (blue color $r > -0.4$; $P < 0.01$) (Fig. 6a). High positive significant correlations ($r > 0.4$, $P < 0.01$) between mean sea level pressure and δ^2H_{trc} were revealed across boreal zone with more pronounced patterns western and central part of HL transect (Fig. 6b). Negative correlations (blue color $r > -0.5$; $P < 0.01$) with winter temperature anomalies versus δ^2H_{trc} are allocated across all boreal sites (Fig. 6c). Winter precipitation (Fig. 6d) spatial patterns show negative significant correlations with the first δ^2H_{trc} principal component for western CAN, central and northeastern Siberia, opposite to positive correlations with δ^2H_{trc} from the Scandinavian sites.

4. Discussion

4.1. Assessment of triple tree-ring stable isotope chronologies

Newly developed $\delta^{18}O_{trc}$ and δ^2H_{trc} for western Canada and available chronologies across the boreal zone show pronounced differences along HL transect. For example, oxygen isotopes in tree rings vary from 19 ‰ for western (CAN), northern and northeastern (TAY, IND) subarctic to 27 ‰ in Scandinavian subarctic (GUT, INA, ILO); and from 23 to 26 ‰ along SIB transect. At the HA transect the $\delta^{18}O_{trc}$ vary from 26.3 to 28.8 ‰.

Even a stronger latitudinal effect is recorded in hydrogen isotope values in tree-ring cellulose showing remarkably depleted values in larch from northeastern subarctic (−171.6 ‰) to more enriched values in Scandinavian pine forests (−94.2 ‰), clearly indicating a continental effect. A cold environment in the subarctic should also favour increased Rayleigh fractionation during hydrological processes in the atmosphere (Dansgaard, 1964), as lower temperatures cause increased rainout events along the water's distillation path from the subtropics to the poles, leading to stronger latitudinal as well as elevational and continental gradients in $\delta^{18}O_{prec}$ and δ^2H_{prec}.

An earlier study by Saurer et al. (2002) showed that average isotope values of 130 trees within the Eurasian subarctic from Norway to Siberia are highly correlated with the modelled isotope distribution of precipitation showing a large east-to-west gradient. These input waters to the soil are modified in the soil by enrichment in ^{18}O as a result of evaporation and in the leaf during transpiration, which is imprinted as a combined isotope signal on photosynthates and cellulose through biochemical fractionation and exchange processes (Roden et al., 2000; Barbour, 2007). In Siberia, the inter-annual variability of winter precipitation $\delta^{18}O$ is closely related to temperature variability and the Arctic and North Atlantic Oscillation (Sidorova et al., 2011; Churakova (Sidorova) et al., 2021, 2022a), while the variability of summer $\delta^{18}O$ appears to be dominated by regional processes involving evaporation and convection (Butzin et al., 2014). Therefore, $\delta^{18}O$ values of tree rings reflect, as a first approximation, average cloud condensation temperatures (Dansgaard, 1964), water origin, cloud cover and showing teleconnection with atmospheric circulation patterns via precipitation, evaporation and condensation processes in the global water cycle (Konecky et al., 2020, 2023).

4.2. Assessment of stable isotopes in tree rings and precipitation water

Our results on site averages (Fig. 3) are consistent and show that annual air temperature is positively correlated with water isotopes and with both $\delta^{18}O_{trc}$ and δ^2H_{trc}, recording ecohydrological signal at the tree level and showing the impact of temperature on stable isotope variability across regions. Similarly, latitude, temperature and related factors are the dominant factors driving large-scale spatial variability in δ^2H_{prec} from the North American arctic and subarctic (Porter et al., 2016, 2022).

The water isotopes could show a link to sunshine through the usual correlation between photosynthesis and transpiration, i.e. increased radiation will promote photosynthesis and in a proportional way transpiration, which in turn influences oxygen and hydrogen isotope fractionation. Loader et al. (2013) reported on the impact of summer sunshine duration on pine tree-ring $\delta^{13}C$ from Sweden, characterizing it as an indirect driver to isotopic fractionation in this study site. Namely, a high coherence was revealed between temperature and sunshine duration over the past centuries, however this relationship was not stable over the past millennia.

Due to low temperatures and permafrost availability in the northeastern part of the subarctic belt, water loss and drought is not yet as largely expressed in stable isotope values compared to the European forest ecosystems (Saurer et al., 2002, 2004, 2014, 2016). There are no clearly increasing trends in recent decades neither in $\delta^{13}C$ or $\delta^{18}O$ chronologies, which would be a sign of increasing drought stress.

4.3. Permafrost thaw and linkage to circulation patterns

Decreasing $\delta^{13}C$ trends were observed mainly for the HL transect in western Canada and northeastern Siberia, which can be explained by an earlier start of the vegetation period in spring and the increased use of precipitation water stored in the soil from autumn of the previous year and early snow melt water utilized by trees during early spring and summer. Thus, an earlier start of the vegetation period could lead to tree-ring formation during a period with higher water availability, resulting in a stronger isotopic fractionation and ^{13}C depletion (Knorre et al., 2010).

The $\delta^{18}O_{trc}$ declining trends for Scandinavian sites can be explained by the impact of the North Atlantic Oscillations, which is in line with the study by Gagen et al. (2016). Decreasing $\delta^{13}C_{trc}$ and δ^2H_{trc} trends along with increasing $\delta^{18}O_{trc}$ trends from western CAN and northeastern TAY and IND can be explained by increasing water availability for trees due to thawing of permafrost during hot and dry summers.

The observed heterogeneous response of trees from the Canadian and Siberian subarctic can be related to ecohydrological changes caused by thawing of permafrost. Its melted water can be used as an additional water source for trees in the Siberian subarctic under warm and dry climate conditions (Sugimoto et al., 2002; Saurer et al., 2016; Churakova (Sidorova) et al., 2016), which is, however, missing in Scandinavian forests.

Fig. 5. Gridded correlation summary plot showing only significant ($P < 0.05$) Pearson correlation coefficients between stable isotope chronologies (left vertical panel from light green to orange) for hydrogen (δ^2H_{trc}, *light green color*), for carbon ($\delta^{13}C_{trc}$, *yellow color*) and for oxygen ($\delta^{18}O_{trc}$, *orange color*) (a) versus average monthly air temperature from September of the previous year to August of the current one; (b) sunshine duration; (c) precipitation; (d) relative humidity and (e) vapor pressure deficit (VPD) for each study site. Positive significant correlations are marked *in a red*, while negative correlations are *in a blue color*. The names for the abbreviations of the sites are listed in Table 1.

4.4. Site- and species-specific differences

Trends divergency can also be related to species-specific (deciduous versus evergreen tree species) differences and response to climatic and eco-physiological changes. Arosio et al. (2020) showed that $\delta 2H_{trc}$ in deciduous tree-ring larch cellulose values from high-elevated sites in the Swiss Alps are more depleted compared to evergreen pine. This difference in hydrogen isotope values was explained by a faster metabolism of the deciduous compared to evergreen tree species. In the boreal zone, deciduous trees, however, grow under extremely cold climate conditions, on soil covered by continuous permafrost. Thus, the highly depleted hydrogen values can be related to cold air temperature and depleted ^{2}H and ^{18}O-source water used by trees, including thawed permafrost water during hot and dry summers.

Therefore, site-specific (e.g., geological location, relief, hydrology) and species-specific (e.g., deciduous vs. evergreen tree species, depth of roots) differences in response to recent and past climatic changes should be taken into consideration for a large-scale analysis and modelling approaches.

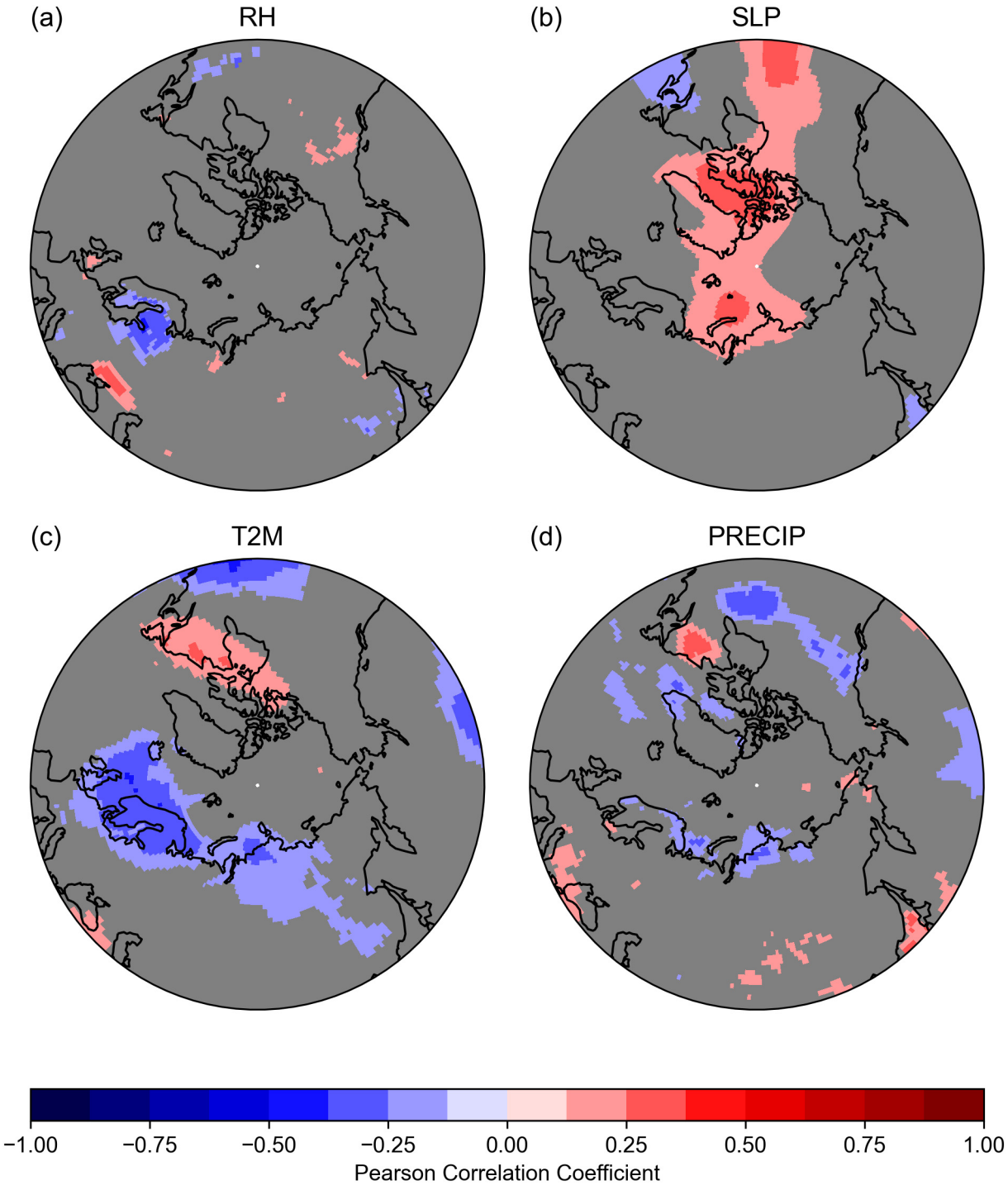

Fig. 6. The first principal component of $\delta^{2}H_{trc}$ versus winter January–February (JF): (a) relative humidity; (b) sea level pressure (SLP); (c) surface air temperature at 2 m (T2M); and (d) precipitation over the period from 1901 to 2000. Negative values of Pearson correlations are marked in a blue color, while positive (in a red color) at the level of significance ($P < 0.01$).

4.5. Impact of climate parameters on triple stable isotopes in tree-ring cellulose

Solar irradiation and its seasonal distribution play an important role for trees in terms of photosynthesis, carbohydrate production and subsequently carbon isotope ratios in organic matter. Increasing photosynthetically active radiation in general results in less negative $\delta^{13}C$ values, particularly when water is not limiting (Farquhar et al., 1989). Our findings show a strong link between tree-ring carbon, but also oxygen and hydrogen stable isotopes and summer sunshine duration during the growth season.

Besides well-known $\delta^{13}C_{trc}$ and $\delta^{18}O_{trc}$, the less investigated $\delta^{2}H_{trc}$ shows negative correlations with sunshine duration during autumn of the previous year and winter of the current year. Such a relationship could be related to the lack of light during polar nights at HL sites (> 60° N) and lack of needles in larch trees to produce photosynthates in a cold environment. Indirect effects might also arise as a high amount of winter sunshine means persistent high-pressure systems with low precipitation, therefore negatively affecting snow accumulation, which is an important water source after snow melt.

A decrease of incoming solar irradiation is also observed during autumn and winter months in western part of the boreal zone, where evergreen species are growing. These trees can potentially produce photoassimilates and transform them into organic matter when the soil is not yet frozen and the air temperature is around +5 °C (temperature threshold, Körner, 2021), and show significant correlation with stable isotopes.

The hydrological regime of Northern Hemispheric boreal forests is rather complex and represents a strong sinusoidal seasonal course of water isotopes imprinted in precipitation ($\delta^{18}O_{prec}$ and $\delta^{2}H_{prec}$), reflecting the cloud condensation temperatures. Uptake of winter precipitation is possible in the warming spring and summer months after snowmelt and thawing of active soil layer. This is confirmed by significant correlations between tree-ring $\delta^{18}O_{trc}$ values and winter-spring air temperatures. Oxygen isotopes in organic matter are modified by variation in the isotopic composition of source water, which is closely related to that of precipitation and soil water (though modified by evaporation at the soil surface) (Voronin et al., 2012; Saurer et al., 2016).

Winter air temperature changes are captured by Scandinavian trees, while winter moisture changes by Siberian conifers, which could be linked to Arctic Oscillation patterns via winter-spring relative humidity and precipitation variability. Our earlier study for the Siberian site (Taimyr Peninsula) showed an impact of Arctic Oscillation during spring on the stable oxygen variability over the past millennia (Sidorova et al., 2011; Churakova (Sidorova) et al., 2021), which may be responsible for drought summers in recent decades. In contrast, the impact of the North Atlantic summer storms may influence Scandinavian conifer trees by bringing moisture conditions (Gagen et al., 2016).

Heterogeneous patterns in relative humidity highlight wet conditions for Scandinavia opposite to drier conditions in western Canada, central and northeastern Siberia. The SSP1–2.6 scenario projected by Balting et al. (2021) showed that the most affected areas, in the context of warming, among others are the Central North America, Siberia and Central Asia. Temperature increase in general will lead to overall drier conditions during summer in the future, which is in line with our findings for the boreal zone.

5. Conclusion

The triple carbon, oxygen and hydrogen isotopes can provide comprehensive information about several climate factors not only during summer but also during winter, spring and autumn. This is hardly possible to reveal from classical tree-ring proxies from the boreal conifers, like tree-ring width and latewood density. The interpretation of results for these regions with their complex hydrology, however, is not straight-forward due to often mixed signals recorded in trees. Mechanistic modelling of isotope ratios may help in determining more clearly the importance of the different climate variables on the observed isotope changes (Barichivich et al., 2021; Siegwolf et al., 2021, 2022).

Our results show the importance of temperature, moisture and sunshine duration changes across the boreal forest zone. Changes in drought are closely associated with the combined changes in temperature, precipitation and evapotranspiration, and are more important in the regions without permafrost (e.g., Scandinavian subarctic), which is a buffer for water availability and additional water access for Siberian conifer trees (Sugimoto et al., 2002; Sidorova et al., 2009).

The observed heterogeneity in climate response, however, can be explained by site- and species-specific differences between evergreen trees (e.g., *Pinus* in Scandinavia and *Picea* in western Canada) versus deciduous species (e.g., *Larix* in Siberia).

The usage of the triple isotope approaches can expand our knowledge beyond that of traditional summer air temperature reconstructions and will help to improve ecohydrological reconstructions over the past millennia.

CRediT authorship contribution statement

OVC (S), MS, RS - Conceptualization; TJP, MS, MW - Data curation; all authors-Formal analysis; Funding acquisition; Investigation; OVS(S), MS, RS, MVF, VVB, AVK, AAK, TVT, VSM - Methodology; OVC(S), TVT, VSM, AVK, VVB - Project administration; OVC(S), MS, RS, NNK, EAV, AVK - Resources; OVC(S), MSZ, MW, Software; OVC(S), MS Supervision; OVC(S), TJP, MSZ, MW, MS - Validation; OVC(S), MSZ, MW - Visualization; All authors - Roles/Writing - original draft; All authors- Writing - review & editing.

Data availability

https://doi.org/10.5281/zenodo.7442809; https://github.com/mikewellmeansme/trs-isotopes-analyser

Declaration of competing interest

The authors declare that they have no known competing financial interests or personal relationships that could have appeared to influence the work reported in this paper.

Acknowledgements

This work was supported by the Russian Science Foundation (RSF), grant number 21-17-00006, “Hydrogen isotopes and deuterium excess (d-excess) in conifer tree-ring cellulose as indicator of extreme eco-hydrological changes in boreal forests (ECO-HYDROTREE)”.

We thank two reviewers for their constructive and valuable suggestions.

References

Abaimov, A.P., Bondarev, A.I., Ziryanova, O.A., Shitova, C.A., 1997. Polar forest of Krasnoyarsk region. Nauka, Sib. Enterprise RAS, Novosibirsk 208 pp.

Apps, M.J., Shvidenko, A.Z., Vaganov, E.A., 2006. Boreal Forests and the Environment: A Foreword, Mitigation and Adaptation Strategies for Global Change. 11(1), pp. 1–4.

Arosio, T., Ziehmer-Wenz, M.M., Nicolussi, K., Schlüchter, C., Leuenberger, M.C., 2020. Larch cellulose shows significantly depleted hydrogen isotope values with respect to evergreen conifers in contrast to oxygen and carbon isotopes. Front. Earth Sci. 8, 523073. https://doi.org/10.3389/feart.2020.523073.

Arosio, T., Ziehmer-Wenz, M.M., Nicolussi, K., Schlüchter, C., Leuenberger, M.C., 2021. Investigating masking effects of age trends on the correlations among tree-ring proxies. Forests 12, 1523. https://doi.org/10.3390/f12111523.

Balting, D.F., Agha Kouchak, A., Lohmann, G., et al., 2021. Northern Hemisphere drought risk in a warming climate. Clim. Atmos. Sci. 4, 61 10.1038.

Barber, V.A., Juday, G.P., Finney, B.P., 2000. Reduced growth of alaskan white spruce in the twentieth century from temperature-induced drought stress. Nature 405, 668–673.

Barbour, M.M., 2007. Stable oxygen isotope composition of plant tissue: a review. Funct. Plant Biol. 34, 83–94.

Barichivich, J., Peylin, P., Launois, T., Daux, V., Risi, C., Jeong, J., Luyssaert, S., 2021. A triple tree-ring constraint for tree growth and physiology in a global land surface model. Biogeosciences 18, 3781–3803. https://doi.org/10.5194/bg-18-3781-2021.

Biskaborn, B.K., Smith, S.L., Noetzli, J., et al., 2019. Permafrost is warming at a global scale. Nat. Commun. 10, 264. https://doi.org/10.1038/s41467-018-08240-4.

Boettger, T., Haupt, M., Knöller, K., Weise, S.M., Waterhouse, J.S., Rinne, K.T., ... Schleser, G.H., 2007. Wood cellulose preparation methods and mass spectrometric analyses of δ13C, δ18O, and nonexchangeable δ^2H values in cellulose, sugar, and starch: an interlaboratory comparison. Anal. Chem. 79 (12), 4603–4612.

Boike, J., Kattenstroth, B., Abramova, K., et al., 2013. Baseline characteristics of climate, permafrost and land cover from a new permafrost observatory in the Lena Rive Delta, Siberia (1998–2011). Biogeosciences 10, 2105–2128.

Bonan, B., 2008. Forests and climate change: forcings, feedbacks, and the climate benefits of forests. Science, 1444–1449 https://doi.org/10.1126/science.1155121.

Bowden, W.B., 2010. Climate change in the Arctic –permafrost, thermokarst, and why they matter to the non-Arctic world. Geogr. Compass 4, 1553–1566.

Bowen, G.J., Revenaugh, J., 2003. Interpolating the isotopic composition of modern meteoric precipitation. Water Resour. Res. 39 (10), 1299 10.129/2003WR002086.

Briffa, K., Schweingruber, F., Osborn, T.J., Shiyatov, S.G., Vaganov, E.A., 1998. Reduced sensitivity of recent tree-growth to temperature at northern high latitudes. Nature 391 (6668), 678–682.

Butzin, M., Werner, M., Masson-Delmotte, V., Risi, C., Frankenberg, C., Gribanov, K., Jouzel, J., Zakharov, V.I., 2014. Variations of oxygen-18 in West Siberian precipitation during the last 50 years. Atmos. Chem. Phys. 14, 5853–5869.

Cable, J.M., Ogle, K., Bolton, R.W., et al., 2014. Permafrost thaw affects boreal deciduous plant transpiration through increased soil water, deeper thaw and warmer soil. Ecohydrology 7 (3), 982–997. https://doi.org/10.1002/eco.1423.

Churakova (Sidorova), O.V., Shashkin, A.V., Siegwolf, R., Spahni, R., Launois, T., Saurer, M., Bryukhanova, M.V., Benkova, A.V., Kupzova, A.V., Vaganov, E.A., Peylin, P., Masson-Delmotte, V., Roden, J., 2016. Application of eco-physiological models to the climatic interpretation of δ^{13}C and δ^{18}O measured in Siberian larch tree-rings. Dendrochronologa 39, 51–59. https://doi.org/10.1016/j.dendro.2015.12.008.

Churakova (Sidorova), O.V., Fonti, M.V., Saurer, M., Guillet, S., Corona, S., Fonti, P., Myglan, V.S., Kirdyanov, A.V., Naumova, O.V., Ovchinnikov, D.V., Shashkin, A.V., Panyushkina, I.P., Büntgen, U., Hughes, M.K., Vaganov, E.A., Siegwolf, R.T.W., Stoffel, M., 2019. Siberian tree-ring and stable isotope proxies as indicators of temperature and moisture changes after major stratospheric volcanic eruptions. Clim. Past 15, 685–700. https://doi.org/10.5194/cp-15-685-2019.

Churakova (Sidorova), O.V., Corona, C., Fonti, M., Guillet, S., Saurer, M., Siegwolf, R.T.W., Stoffel, M., Vaganov, E.A., 2020. Recent atmospheric drying in Siberia is not unprecedented over the last 1500 years. Sci. Rep. 10 14(1) https://www.nature.com/articles/s41598-020-71656-w.

Churakova (Sidorova), O.V., Myglan, V.S., Fonti, M.V., Saurer, M., 2021a. Isotopic responses to dry and wet episodes as captured in tree rings of southern Altai relict forests. Eur. J. For. Res. 140, 527–535. https://doi.org/10.1007/s10342-020-01338-9.

Churakova (Sidorova), O.V., Siegwolf, R.T.W., Fonti, M.V., Vaganov, E.A., Saurer, M., 2021b. Spring Arctic Oscillation as a trigger of summer drought in Siberian subarctic over the past 1494 years. Sci. Rep. 11, 19010. https://doi.org/10.1038/s41598-021-97911-2.

Churakova (Sidorova), O.V., Fonti, M.V., Barinov, V.V., Zharkov, M.S., Taynik, A.V., Trushkina, T.V., Bondarev, A.I., Kirdyanov, A.V., Arzac, A., Saurer, M., 2022a. Towards the third millennium changes in Siberian triple tree-ring stable isotopes. Forests 13 (6), 934. https://doi.org/10.3390/f13060934.

Churakova (Sidorova), O.V., Porter, T.J., Kirdyanov, A.V., Myglan, V.S., Fonti, M.V., Vaganov, E.A., 2022b. Stable isotopes in tree rings of boreal forests. In: Siegwolf, R.T.W., Brooks, J.R., Roden, J., Saurer, M. (Eds.), Stable Isotopes in Tree Rings. Tree Physiology. 8. Springer, Cham, pp. 581–603. https://doi.org/10.1007/978-3-030-92698-4_20.

Churakova-Sidorova, O.V., Myglan, V.S., Fonti, M.V., et al., 2022. Modern aridity in the Altai-Sayan mountain range derived from multiple millennial proxies. Sci. Rep. 12, 7752. https://doi.org/10.1038/s41598-022-11299-1.

Dansgaard, W., 1964. Stable isotopes in precipitation. Tellus 16 (4), 436–468. https://doi.org/10.1111/j.2153-3490.1964.tb00181.x.

D'Arrigo, R.D., Wilson, R., Liepert, B., Cherubini, P., 2008. On the 'divergence problem' in northern forests: a review of the tree-ring evidence and possible causes. Glob. Planet. Chang. 60, 289–305.

Farquhar, G.D., Ehleringer, J.R., Hubick, K.T., 1989. Carbon isotope discrimination and photosynthesis. Annu. Rev. Plant Phisiol. Plant Mol. Biol. 40, 503–537.

Farquharson, L.M., Romanovsky, V.E., Cable, W.L., Walker, D.A., Kokelj, S.V., Nicolsky, D., 2019. Climate change drives widespread and rapid thermokarst development in very cold permafrost in the Canadian High Arctic. Geoph. Res. Lett. 46 (12), 6681–6689. https://doi.org/10.1029/2019GL082187.

Francey, R.J., et al., 1999. A 1000-year high precision record of δ^{13}C in atmospheric CO_2. TellusSer. B 51, 170–193.

Gagen, M., McCarroll, D., Jalkanen, R., Loader, N.J., Robertson, I., Young, G.H.F., 2012. A rapid method for the production of robust millennial length stable isotope tree-ring series for climate reconstruction. Glob. Planet. Chang. https://doi.org/10.1016/j.gloplacha.2011.1011.1006.

Gagen, M., et al., 2016. North Atlantic summer storm tracks over Europe dominated by internal variability over the past millennium. Nat. Geosci. 9 (8), 630–635.

Garnello, A., Marchenko, S., Nicolsky, D., Romanovsky, V., Ledman, J., Celis, G., et al., 2021. Projecting permafrost thaw of sub-Arctic tundra with a thermodynamic model calibrated to site measurements. J. Geophys. Res. Biogeosci. 126, e2020JG006218. https://doi.org/10.1029/2020JG006218.

Gennaretti, F., Huard, D., Naulier, M., Savard, M., Bégin, C., Arseneault, D., Guiot, J., 2017. Bayesian multiproxy temperature reconstruction with black spruce ring widths and stable isotopes from the northern Quebec taiga. Clim. Dyn. 49, 4107–4119. https://doi.org/10.1007/s00382-017-3565-5.

Harris, I., Osborn, T.J., Jones, P., Lister, D., 2020. Version 4 of the CRU TS monthly high-resolution gridded multivariate climate dataset. Sci Data 7, 109. https://doi.org/10.1038/s41597-020-0453-3.

Helbig, N., Mott., R., van Herwijnen, A., Winstral, A., Jonas, T., 2017. Parameterizing surface wind speed over complex topography. J. Geophys. Res. Atmos. 122, 651–667. https://doi.org/10.1002/2016JD025593.

Hersbach, H., Bell, B., Berrisford, P., Hirahara, S., Horányi, A., Muñoz-Sabater, J., et al., 2020. The ERA5 global reanalysis. Q. J. R. Meteorol. Soc. 146, 1999–2049. https://doi.org/10.1002/qj.3803.

Hilasvuori, E., 2011. Environmental and climatic dependences of stable isotopes in tree rings on different temporal scales. Department of Environmental sciences, Faculty of biological and environmental sciences, University of Helsinki.

Kimak, A., Leuenberger, M., 2015. Are carbohydrate storage strategies of trees traceable by early–latewood carbon isotope differences? Trees 29, 859–870. https://doi.org/10.1007/s00468-015-1167-6.

Kirdyanov, A.V., Treydte, K.S., Nikolaev, A., Helle, G., Schleser, G.H., 2008. Climate signals in tree-ring width, density an δ^{13}C from larches in Eastern Siberia (Russia). Chem. Geol. 252, 31–41. https://doi.org/10.1016/j.chemgeo.2008.01.023.

Knorre, A.A., Kirdyanov, A.V., Vaganov, E.A., 2006. Climatically induced interannual variability in aboveground production in forest-tundra and northern taiga of Central Siberia. Oecologia 147, 86–95. https://doi.org/10.1007/s00442-005-0248-4.

Knorre, A.A., Siegwolf, R., Saurer, M., Sidorova, O.V., Vaganov, E.A., Kirdyanov, A.V., 2010. Twentieth century trends in tree rings stable isotopes (δ^{13}C and δ^{18}O) of *Larix sibirica* under dry conditions in the forest steppe in Siberia. Geophys.Res.Biogeosci. 115, G03002. https://doi.org/10.1029/2009JG000930 1-12.

Konecky, B.L., McKay, N.P., Churakova (Sidorova), O.V., Comas-Bru, L., Dassié, E., DeLong, K., Falster, G., Fischer, M., Jones, M.D., Jonkers, L., Kaufman, D.S., Leduc, G., Managave, S., Martrat, B., Opel, T., Orsi, A.J., Partin, J.W., Sayani, H.R., Thomas, E.K., Thompson, D.M., Tyler, J.J., Abram, N.J., Atwood, A.R., Conroy, J.L., Kern, Z., Porter, T.J., Stevenson, S.L., von Gunten, L., the Iso2k Project, Members., 2020. The Iso2k Database: A global compilation of paleo-δ^{18}O and δ2H records to aid understanding of Common Era climate. Earth System Science Data (12),, 2261–2288. https://doi.org/10.1029/2019GL082187.

Konecky, B.L., McKay, N.P., Churakova (Sidorova), O.V., Comas-Bru, L., Dassié, E., DeLong, K., Falster, G., Fischer, M., Jones, M.D., Jonkers, L., Kaufman, D.S., Leduc, G., Managave, S., Martrat, B., Opel, T., Orsi, A.J., Partin, J.W., Sayani, H.R., Thomas, E.K., Thompson, D.M., Tyler, J.J., Abram, N.J., Atwood, A.R., Conroy, J.L., Kern, Z., Porter, T.J., Stevenson, S.L., von Gunten, L., Iso2k Project Members, 2023. Temperature-driven changes in the global water cycle during the Common Era. Nat. Geosci. (under review).

Kononov, Y., Friedrich, M., Boettger, T., 2009. Regional summer temperature reconstruction in the Khibiny low mountains (Kola Peninsula, NW Russia) by means of tree-ring width during the last four centuries. Arct. Antarct. Alp. Res. 4 (4), 460–468. https://doi.org/10.1657/1938-4246-41.4.460.

Körner, Ch., 2021. The cold range limit of trees. Trends Ecol.Eval. 979–989.

Lehmann, M.M., Vitali, V., Schuler, P., Leuenberger, M., Saurer, M., 2021. More than climate: hydrogen isotope ratios in tree rings as novel plant physiological indicator for stress conditions. Dendrochronologia 65, 125788.

Loader, N.J., Robertson, I., Barker, A.C., Switsur, V.R., Waterhouse, J.S., 1997. Improved technique for the batch processing of small whole wood samples to alpha-cellulose. Chem. Geol. 136, 313–317.

Loader, N.J., Helle, G., Los, S.O., Lehmkuhl, F., Schleser, G.H., 2010. Twentieth-century summer temperature variability in the southern Altai Mountains: a carbon and oxygen isotope study of tree-rings. The Holocene 20 (7). https://doi.org/10.1177/0959683610369507.

Loader, N.J., Young, G.H.F., Grudd, H., McCarroll, D., 2013. Stable carbon isotopes from Torneträsk, norther Sweden provide a millennial length reconstruction of summer sunshine and its relationship to Arctic circulation quat. Sci. Rev. 62, 97–113.

Loader, N.J., Street-Perrott, F.A., Daley, T.J., Hughes, P.D.M., Kimak, A., Levanič, T., et al., 2015. Simultaneous determination of stable carbon, oxygen, and hydrogen isotopes in cellulose. Anal. Chem. 87 (1), 376–380. https://doi.org/10.1021/ac502557x.

McCarroll, D., Loader, N.J., 2004. Stable isotopes in tree rings. Quat. Sci. Rev. 23 (7–8), 771–801.

Naulier, M., Savard, M.M., Bégin, C., Gennaretti, F., Arseneault, D., Marion, J., Nicault, A., Bégin, Y., 2015. A millennial summer temperature reconstruction for northeastern Canada using oxygen isotopes in subfossil trees. Clim. Past 11, 1153–1164. https://doi.org/10.5194/cp-11-1153-2015.

Obu, J., Westermann, S., Bartsch, A., et al., 2019. Northern hemisphere permafrost map based on TTOP modelling for 2000–2016 at 1 km2 scale. Earth-Sci.Rev. 193, 299–316. https://www.sciencedirect.com/science/article/pii/S0012825218305907.

Porter, T.J., Pisaric, M.F.J., 2011. Temperature–growth divergence in white spruce forests of Old Crow Flats, Yukon Territory, and adjacent regions of northwestern North America. Glob. Chang. Biol. 17, 3418–3430.

Porter, T.J., Pisaric, M.F.J., Kokelj, S.V., Edwards, T.W.D., 2009. Climate signals in δ^{13}C and δ^{18}O of tree-rings from white spruce in the Mackenzie Delta region, northern Canada. Arct. Antarct. Alp. Res. 41, 497–505.

Porter, T.J., Pisaric, M.F.J., Kokelj, S.V., deMontigny, P., 2013. A ring-width-based reconstruction of June–July minimum temperatures since AD 1245 from white spruce stands in the Mackenzie Delta region, northwestern Canada. Quat. Res. 80, 167–179.

Porter, T.J., Pisaric, M.F.J., Field, R., Kokel, S.V., Edwards, T.W.D., deMontigny, P., Healy, R., LeGrande, A., 2014. Spring-summer temperatures since AD 1780 reconstructed from stable oxygen isotope ratios in white spruce tree-rings from the Mackenzie Delta, northwestern Canada. Clim. Dyn. 42, 771–785.

Porter, T.J., Froese, D.G., Feakins, S.J., Bindeman, I., Mahony, M.E., Pautler, B.G., Reichart, G.-J., Sanborn, P.T., Simpson, M.J., Weijers, J.W.H., 2016. Multiple water isotope proxy reconstruction of extremely low last glacial temperatures in Eastern Beringia (Western Arctic). Quat. Sci. Rev. 137, 113–125.

Porter, T.J., Anhäuser, T., Halfar, J., Keppler, F., Csank, A.Z., Williams, C.J., 2022. Canadian Arctic neogene temperatures reconstructed from hydrogen isotopes of lignin-methoxy

groups from sub-fossil wood. Paleoceanogr.Paleoclimatol. 37 (2). https://doi.org/10.1029/2021PA004345.

Roden, J.S., Lin, G., Ehleringer, J.R., 2000. A mechanistic model for interpretation of hydrogen and oxygen isotopic ratios in tree-ring cellulose. Geochem.Cosmochim.Acta 64 (1), 21–35.

Saurer, M., Schweingruber, F., Vaganov, E.A., Shiyatov, S.G., Siegwolf, R., 2002. Spatial and temporal oxygen isotope trends at the northern tree-line in Eurasia. Geophys. Res. Lett. 29 (9), 1296–1300. https://doi.org/10.1029/2001GL013739.

Saurer, M., Siegwolf, R., Schweingruber, F.H., 2004. Carbon isotope discrimination indicates improving water-use efficiency of trees in northern Eurasia over the last 100 years. Glob. Chang. Biol. 10, 2109–2121.

Saurer, M., Kirdyanov, A.V., Prokushkin, A.S., Rinne, K.T., Siegwolf, R.T.W., 2016. The impact of an inverse climate-isotope relationship in soil water on the oxygen-isotope composition of *Larix gmelinii* in Siberia. New Phyt. 209, 955–964.

Saurer, M., Spahni, R., Frank, D.C., Joos, F., Leuenberger, M., Loader, N.J., McCarroll, D., Gagen, M., Poulter, B., Siegwolf, R.T., Andreu-Hayles, L., Boettger, T., Dorado Linan, I., Fairchild, I.J., Friedrich, M., Gutierrez, E., Haupt, M., Hilasvuori, E., Heinrich, I., Helle, G., Grudd, H., Jalkanen, R., Levanic, T., Linderholm, H.W., Robertson, I., Sonninen, E., Treydte, K., Waterhouse, J.S., Woodley, E.J., Wynn, P.M., Young, G.H., 2014. Spatial variability and temporal trends in water-use efficiency of European forests. Glob. Chang. Biol. 20, 3700–3712.

Schuler, P., Cormier, M.-A., Werner, R.A., Buchmann, N., Gessler, A., Vitali, V., Saurer, M., Lehmann, M.M., 2022. A high-temperature water vapor equilibration method to determine non-exchangeable hydrogen isotope ratios of sugar starch and cellulose. Plant Cell Environ. 45 (1), 12–22. https://doi.org/10.1111/pce.14193.

Sidorova, O.V., Siegwolf, R., Saurer, M., Naurzbaev, M.M., Vaganov, E.A., 2008. Isotopic composition ($\delta^{13}C$, $\delta^{18}O$) in Siberian tree-ring chronology. Geophys. Res. Biogeosci. 113, G02019. https://doi.org/10.1029/2007JG000473.

Sidorova, O.V., Siegwolf, R., Saurer, M., Shashkin, A.V., Knorre, A.A., Prokushkin, A.S., Vaganov, E.A., Kirdyanov, A.V., 2009. Do centennial tree-ring and stable isotope trends of *Larix gmelinii* (Rupr.) indicate increasing water shortage in the Siberian north? Oecologia 161 (4), 825–835. https://link.springer.com/article/10.1007/s00442-009-1411-0.

Sidorova, O.V., Siegwolf, R., Saurer, M., Naurzbaev, M., Shashkin, A.V., Vaganov, E.A., 2011. Spatial patterns of climatic changes in the Eurasian north reflected in Siberian larch tree-ring parameters and stable isotopes. Glob. Chang. Biol. 16, 1003–1018. https://doi.org/10.1111/j.1365-2486.2009.02008.x.

Sidorova, O.V., Saurer, M., Andreev, A., Fritzsche, D., Opel, T., Naurzbaev, M., Siegwolf, R., 2013a. Is the 20th century warming unprecedented in the Siberian north? Quat. Sci. Rev. 73, 93–102. https://doi.org/10.1016/j.quascirev.2013.05.015.

Sidorova, O.V., Siegwolf, R., Myglan, V.S., Loader, N.J., Helle, G., Saurer, M., 2013b. The application of tree-rings and stable isotopes for reconstructions of climate conditions in the Altai-Sayan Mountain region. Clim. Chang. https://doi.org/10.1007/s10584-013-0805-5.

Sidorova, O.V., Saurer, M., Myglan, V.S., Eichler, A., Schwikowski, M., Kirdyanov, A.V., Bryukhanova, M.V., Gerasimova, O.V., Kalugin, I., Daryin, A., Siegwolf, R., 2012. A multi-proxy approach for revealing recent climatic changes in the Russian Altai. Clim. Dyn. 38 (1–2), 175–188.

Siegwolf, R., Lehmann, M., Goldsmith, G., Churakova (Sidorova), O.V., Mirande-Ney, C., Timoveeva, G., Weigt, R., Saurer, M., 2021. Revisiting the dual carbon and oxygen isotope model for understanding plant functional response to environment. https://doi.org/10.22541/au.163844646.68129291/v1 pre-prtint.

Siegwolf, R.T.W., Brooks, J.R., Roden, J., 2022. Stable isotopes in tree rings inferring physiological, climatic and environmental responses stable isotope in tree rings, p. 773. https://doi.org/10.1007/978-3-030-92698-4.

Slivinski, L.C., et al., 2019. Towards a more reliable historical reanalysis: improvements for version 3 of the twentieth century reanalysis system. Quart. J. Roy. Meteor. Soc. 145, 2876–2908. https://doi.org/10.1002/qj.3598.

Slivinski, L.C., 2021. An Evaluation of the performance of the twentieth century reanalysis version 3. J. Clim. 34 (4), 1417–1438. https://doi.org/10.1175/JCLI-D-20-0505.1.

Smith, T., Traxl, D., Boers, N., 2022. Empirical evidence for recent global shifts in vegetation resilience. Nat. Clim. Chang. 12, 477–484. https://doi.org/10.1038/s41558-022-01352-2.

Soja, A.J., Tchebakova, N.M., French, N.H.F., Flannigan, M.D., Shugart, H.H., Stocks, B.J., Sukhinin, A.I., Parfenova, E.I., Chapin, F.S., Stackhouse, P.W., 2007. Climate induced boreal forest change: predictions versus current observations. Glob. Planet. Chang. 56, 274–296.

Sugimoto, A., Yanagisawa, N., Naito, D., Fujita, N., Maximov, T.C., 2002. Importance of permafrost as a source of water for plants in East Siberian taiga. Ecol. Res. 17 (4), 493–503. https://doi.org/10.1046/j.1440-1703.2002.00506.x.

Tartakovsky, V.A., Voronin, V.I., Markelova, A.N., 2012. External forcing factor reflected in the common signals of ^{18}O-tree-ring series of Larix sibirica Ledeb. in the Lake Baikal region. Dendrochronologia 30, 199–208. https://doi.org/10.1016/j.dendro.2011.08.004.

Taynik, A.V., Myglan, V.S., Barinov, V.V., Oidupaa, O.C., Churakova (Sidorova), O.V., 2023. **Ancient larch trees in the Tuva Republic, land of the oldest trees in Russia** EcoMont. 7 in press.

Timofeeva, G., 2017. Elucidating the drought response of Scots pine (*Pinus sylvestris* L.) using stable isotopes. ETH Zürich https://doi.org/10.3929/ethz-b-000274056 PhD Thesis.

Vaganov, E.A., Hughes, M.K., Shashkin, A.V., 2006. Growth Dynamics of Conifer Tree Rings: Images of Past and Future Environments. Springer 353 p.

Vitali, V., Martinez-Sancho, E., Treydte, K., Andreu-Hayles, L., Dorado-Linan, I., Gutierrez, E., Helle, G., Leuenberger, M., Loader, N.J., Rinne-Garmston, K.T., Schlesser, G.H., Allen, S., Waterhouse, J.S., Saurer, M., Lehmann, M.M., 2022. The unknown third – hydrogen isotopes in tree-ring cellulose across Europe. Sci. Total Environ. 813, 152281.

Voelker, S.L., Brooks, J.R., Meinzer, F.C., Roden, J., Pazdur, A., Pawelczyk, S., Hartsough, P., Snyder, K., Plavcova, L., Šantrůček, J., 2014. Reconstructing relative humidity from plant $\delta^{18}O$ and δD as deuterium deviations from the global meteoric water line. Ecol. Appl. 24, 960–975.

Voronin, V., Ivlev, A.V., Oskolkov, V., Boettger, T., 2012. Intra-seasonal dynamics in metabolic processes of $^{13}C/^{12}C$ and $^{18}O/^{16}O$ in components of scots pine twigs from southern Siberia interpreted with a conceptual framework based on the carbon metabolism oscillatory model. BMC Plant Biol. 12, 76. https://doi.org/10.1186/1471-2229-12-76.

Waskom, M.L., 2021. Seaborn: statistical data visualization. J.Open Source Softw. 6 (60), 3021. https://doi.org/10.21105/joss.03021.

Weigt, R.B., et al., 2015. Comparison of $\delta^{18}O$ and $\delta^{13}C$ values between tree-ring whole wood and cellulose in five species growing under two different site conditions. Rapid Commun. Mass Spectrom. 29 (23), 2233–2244.

Wilmking, M., Juday, G.P., Barber, V.A., Zald, H.S.J., 2004. Recent climate warming forces contrasting growth responses of white spruce at tree-line in Alaska through temperature thresholds. Glob. Chang. Biol. 10 1724–173.

Woodley, E.J., Loader, N.J., McCarroll, D., Young, G.H.F., Robertson, Y.I., Hearon, T.H.E., Gagen, M.H., 2012. Estimating uncertainty in pooled stable isotope time-series from tree-rings. Chem. Geol. 10, 294–295.

Young, G.H.F., McCarroll, D., Loader, N.J., Gagen, M.H., Kirchhefer, A.J., Demmler, J.C., 2012. Changes in atmospheric circulation and the Arctic Oscillation preserved within a millennial length reconstruction of summer cloud cover from northern Fennoscandia. Clim. Dyn. 39, 495–507. https://doi.org/10.1007/s00382-011-1246-3.

Zandt, M.H., Liebner, S., Welte, C.U., 2020. Thermokarst lakes in a warming world. Trends Microbiol. 28 (9), 769–779. https://doi.org/10.1016/j.tim.2020.04.002.

Zharkov, M.M., Fonti, M.V., Trushkina, T.V., Barinov, V.V., Taynik, A.V., Porter, T., Saurer, M., Churakova (Sidorova), O.V., 2021. Mixed temperature-moisture signal in $\delta^{18}O$ records of boreal conifers from the permafrost zone. MDPI Atmos. 12 (11), 1416. https://doi.org/10.3390/atmos12111416.